RHEOLOGICAL CONTROL OF REACTIVE AND NONREACTIVE PARTICLES

by

LYN ZEMBEREKÇİ

Submitted to the Graduate School of Engineering and Natural Sciences
in partial fulfillment of the requirements for the degree of
Master of Science

Sabanci University
November 2020

RHEOLOGICAL CONTROL OF REACTIVE AND NONREACTIVE PARTICLES

APPROVED BY:

DATE OF APPROVAL: ……

ABSTRACT

RHEOLOGICAL CONTROL OF REACTIVE AND NONREACTIVE PARTICLES

LYN ZEMBEREKÇİ

Materials Science and Nano Engineering, MSc. Thesis, 2020

Thesis Advisor: Assoc. Prof. Dr. Özge Akbulut

Keywords:

Rheology, Dispersion, Cement, Coagulation, Nano Particles, Linear Copolymers

Controlling the shear response of colloidal systems is critical in the ceramics industry as it affects the final properties of the product. In this thesis, reactive cementitious particles and nonreactive ceramic particles were studied and characterized by a colloidal science point of view. In the first part, the formulation of an extrudable, lightweight, high-strength cement-based material that utilizes industrial waste products was achieved. A random grafted copolymer that capitalizes electrostatic repulsion and steric hindrance was the key to control the flow of the particles. In the optimized mixture, high performance was maintained in terms of the compressive strength at 80 MPa and the dry hardened density at 1900 kg/cm^3. According to the American Concrete Institute, this formulation is classified as high-strength (>55 MPa) and lightweight (320–1920 kg/m^3). In the second part, the green machinability of yttria-stabilized zirconia was attained by employing a linear random copolymer. The copolymer was designed to coagulate the system by polymer-polymer bridging and facilitated an innovative ceramic gelcasting approach. The optimized system resulted in a shrinkage of 22.8%, a flexural strength of 149 MPa, and a density of 5.93 g/cm^3. Compared to the values given in the literature; the shrinkage is 20–30%, the flexural strength is 150 MPa, and the theoretical density is 6.07 g/cm^3.

ÖZET

REAKTİF VE REAKTİF OLMAYAN PARTİKÜLLERİN REOLOJI KONTROLÜ

LYN ZEMBEREKÇİ

Malzeme Bilimi ve Nano Mühendislik, Yüksek Lisans Tezi, 2020

Tez Danışmanı: Assoc. Prof. Dr. Özge Akbulut

Anahtar Kelimeler:

Reoloji, Çimento, Kogaülasyon, Nano Partiküller, Kopolimer

Seramik endüstrisinde kolloidal sistemlerin kayma tepkisi ürünün nihai özelliklerini etkilediğinden ötürü kritik bir önem taşımaktadır. Bu tez çalışmasında, reaktif çimento esaslı partiküller ve reaktif olmayan seramik partiküller incelenmiştir ve kolloidal bilimi bakış açısıyla karakterize edilmiştir. Çalışmanın ilk kısmında, endüstriyel atık ürünlerinden elde edilen, ekstrüde edilebilir, hafif agregalı ve yüksek dayanımlı çimento esaslı malzeme formülasyonu elde edilmiştir. Elektrostatik itme ve sterik engel özelliklerinden faydalanan rastgele graftlanmış kopolimer, partiküllerin akışını kontrol etmek için kilit nokta olmuştur. Optimize edilmiş karışımda, 80 MPa basınç dayınımı ve 1900 kg/cm^3 kuru-sertleşmiş yoğunluk çerçevesinde yüksek performans korunmuştur. Amerikan Beton Enstitüsü'ne göre bu formülasyon, yüksek dayanımlı (>55 MPa) ve hafif agregalı (320-1920 kg/m^3) olarak sınıflandırılmıştır. Çalışmanın ikinci kısmında, rastgele doğrusal bir kopolimer kullanarak itriya ile stabilize edilmiş zirkonyanın yaş işlenebilirliği elde edilmiştir. Bu kopolimer, sisteme polimer-polimer köprüleme ile koagülasyon yapması için tasarlanmıştır ve inovatif bir seramik jel kaplama yaklaşımına olanak tanımışır. Optimize edilmiş sistem %22.8'lik büzülme, 149 MPa'lık eğilme dayanımı ve 5.93 g/cm^3'lük yoğunluk değeri göstermiştir. Literatürde verilen değerler ile karşılaştırıldığında; büzülme %20-30, eğilme dayanımı 150 MPa ve yoğunluk 6.07 g/cm^3 olarak görülmektedir.

ACKNOWLEDGEMENTS

This thesis would not have been made possible without the constant support of my family, friends, and professors.

I deeply appreciate my advisor, Prof. Özge Akbulut, for teaching me the importance of being detail-oriented and open-minded to new opportunities, and for being a role model of a successful researcher both in and out of the academic world. Many thanks to my first academic advisor, Prof. Zeynep Başaran Bundur, for introducing me to the research world and for being supportive, way beyond my undergraduate program. I am also thankful to Prof. Mehmet Ali Gülgün for his invaluable guidance, patience, and fun spirit. I greatly appreciate Dr. Omid Akhlaghi for his insight on the experimental work, constant support, and for laying a solid foundation in our research group.

I am so thankful for my loving parents for always putting me as their priority and for helping me with off-campus tasks. I am very grateful for having my close friends; Eda Kırımlı, Mervenaz Şahin, Nargiz Yessengali, Aysoltan Ymamgulyyeva, Ozan Eray Aydın, and Yiğit Alper Atalay by my side and for being a strong support system.

Lastly, I would like to thank each one of my research group and laboratory mates: Gizem Demir, Can Akaoğlu, Wael Ali Aldulaimi, Madineh Rastgoo, Burak Özbek, Arzu Coşgun Ergene, Sirous Khabbaz, Semih Pehlivan, Merve Buldu, Ekin Berksun, Irmak Kayalan, and Aleyna Beste Özhan, for all their help with the laboratory experiments and for being good friends.

To my parents

TABLE OF CONTENTS

LIST OF TABLES

LIST OF FIGURES

LIST OF SYMBOLS AND ABBREVIATIONS

AA	Acrylic Acid
AMPS	2-Acrylamido 2-methylpropane Sulfonic Acid
CM	Control Mixture
DCC	Direct Coagulation Casting
DLS	Direct Light Scattering
FAC	Fly-ash Cenospheres
GPC	Gel Permeation Chromatography
KPS	Potassium Persulfate
Mw	Molecular Weight
NMR	Nuclear Magnetic Resonance
OPC	Ordinary Portland Cement
PEG	Polyethylene Glycol
PSA	Particle Size Analyzer
RMA	Rheology-Modifying Additive
SCM	Supplementary Cementitious Materials
SEM	Scanning Electron Microscope
UTM	Universal Testing Machine
VPA	Vinylphosphonic Acid
YSZ	Yttria-Stabilized Zirconia

CHAPTER 1

INTRODUCTION

1.1. Thesis Overview

I have divided my thesis into three main chapters; the first chapter introduces and links the following chapters together and at the same time serves as an introduction to rheology, specifically concepts pertaining to the presented work.

The second chapter is entirely focused on the formulation of robust extrudable cement-based systems using three main cementitious particles: white cement, silica fume, and fly-ash cenospheres particles. It is also indicative of taking a rheology-based approach to design a formulation for a specific application, in this case, extrusion of cement-based materials. This chapter is collateral to my group's previous research on grafted copolymers additives. The purpose of that was to cater to niche cementitious systems as opposed to the commercially available additives that work only with ordinary Portland cement. The research in this thesis was carried out to further study the compatibility of the grafted copolymers with more cement-based particles.

The third chapter is devoted to the green machinability of nano yttria-stabilized zirconia that was made possible by employing a linear copolymer. I delve into the design of the copolymer, which behaves as a coagulant (flocculant) of nano yttria-stabilized zirconia. I start the discussion by introducing a set of polymers and discussing the underlying polymer chemistry. Then, I relate the polymer chemistry to the behavior of ceramic particles. The connection was made clear by recording a set of different rheological behaviors with every copolymer at different percentages. The results of both of the chapters will be submitted to befitting peer-reviewed journals.

1.2. Thesis Objective

The objective of my thesis is to study the rheological behavior of different particles; reactive, such as cementitious particles, and nonreactive, such as ceramic particles, in relation to colloidal science. At the same time, the purpose was to modify that behavior through an application-based approach by introducing a specifically-designed polymer to the particle systems. Furthermore, testing the materials at every step of the design was crucial to comply with the standards and prove the reliability and reproducibility of the results as well as their comparability to the existing research on the topics.

1.3. Introduction to Rheology

Rheology is the science that studies the flow of materials, originating from the Greek word "*rhein*" meaning "to flow" [1]. Different materials display this rheological behavior differently; for instance, highly viscous materials exhibit a stronger resistance to shear stress/rate than fluid materials. While it is a phenomenon that can be assessed macroscopically, this rheological response is directly related to the type of interaction between the particles on the microstructural level [2]. Recently, material systems have been optimized for different applications using a rheology-based approach to design stable formulations. These systems include but not limited to; additive manufacturing, conventional ceramic processing, modified ceramic processing such as direct coagulation casting and gelation, conventional concrete casting, and modified concrete casting such as self-consolidating concrete [3–7].

A particle-system (suspension) is formed by loading particles into a liquid where they stay suspended or sedimented or coagulated based on the interparticle forces in the system. If they have strong attractive Van der Waals interparticle forces and/or high surface area, then, they agglomerate or precipitate, thereby, increasing the viscosity of the suspension [8]. While in certain instances agglomeration is desirable to achieve a coagulating or gelling effect, it can also result in an unstable suspension. Instability is characterized by the separation of the phases, i.e. liquid-solid phase separation, often utilized in water treatment applications [9]. One way to track the rheological response of a material is by understanding the dispersion of particles in the suspension, which

depends on the loading, the surface properties of particles, and particle-medium interactions [2, 8]. This chapter explores the theory of understanding the dispersion of particles and the mechanisms employed to modify them by modifying their rheology. Furthermore, the chapter underlines the different rheological behaviors of materials and their importance in engineering applications; the next chapters put the theory into the experiment.

1.4. Stability of Colloids and the DLVO Theory

The stability of colloidal particles suspended in a solvent is crucial to avoid undesired agglomeration or sedimentation of particles [10]. Additionally, the higher the stability of the suspension, the higher the solid concentration could be to remain in the flowable state [2, 8]. Orderly structured and highly loaded colloids are necessary for ink formation for additive manufacturing and injection molding applications. The reason is that the obtained experimental density of such inks would be the closest to its theoretical value [4, 5].

Assuming the particles in a suspension are hard spheres and are moving in a Brownian (random) motion. Starting with examining the particles in a medium without any additives, there will be two cases for the initial stability of the suspensions: 1) if they have intrinsically high surface potential, the suspension would be stable due to the predominant electrostatic repulsion. And 2) if the particles are partially/weakly ionic, the van der Waals attraction will be predominant, which exists due to the dipole-dipole interaction between the particles, thus leading to agglomeration as they stick together.

Furthermore, if chemical additives such as dispersants, polyelectrolytes, and salts, frequently used for stabilization, are added to the suspension, the resulting phenomena can be described by the DLVO theory[1] [11]. To elaborate on this theory, we take an example of a partially negatively charged particle, as illustrated in Figure 1. Upon the addition of a positive ion in the solution, these ions adsorb and strongly bond to the surface of the particle forming what is called a stern layer. This strong positivity will attract some negative charges that surround the Stern layer and form the diffuse layer.

[1] Named after Derjaguin, Landau, Verwey, and Overbeek

However, the diffuse layer is still predominately positive, which is clear by the drop in the potential energy shown in Figure 1. Together, the Stern and the diffuse layers are referred to as the double layer on a colloidal particle. Thus, a potential exists between the boundaries of these two layers, known as the Stern potential. Another potential known as the Zeta potential is created at the slipping plane that exists between the diffuse layer and the medium. The interaction among the double layers of the particles that are approaching each other in the solution determines the stability. In this case, the DLVO theory shows that the total potential energy is equal to the sum of the van der Waals attraction and the double layer repulsion as, $V_T = V_A + V_R$. The repulsion is taken as positive and the attraction as negative, if, $V_T > 0$, V_R is predominant and the colloid is stable. If $V_T < 0$, V_A is predominant, the colloid is unstable, and that causes particles to agglomerate.

Similarly, if the diffuse layer is large, then, the double layer repulsion and the zeta potential will be higher. Therefore, the zeta potential is an accurate indicator of colloid stability and is often experimentally measured [12]. Concerning rheology, the described particle-particle interaction, based on their surface features, reins the behavior, and directly affects the viscosity [2]. Stable suspensions with high zeta potential values have lower viscosity values as oppose to unstable agglomerated ones [13].

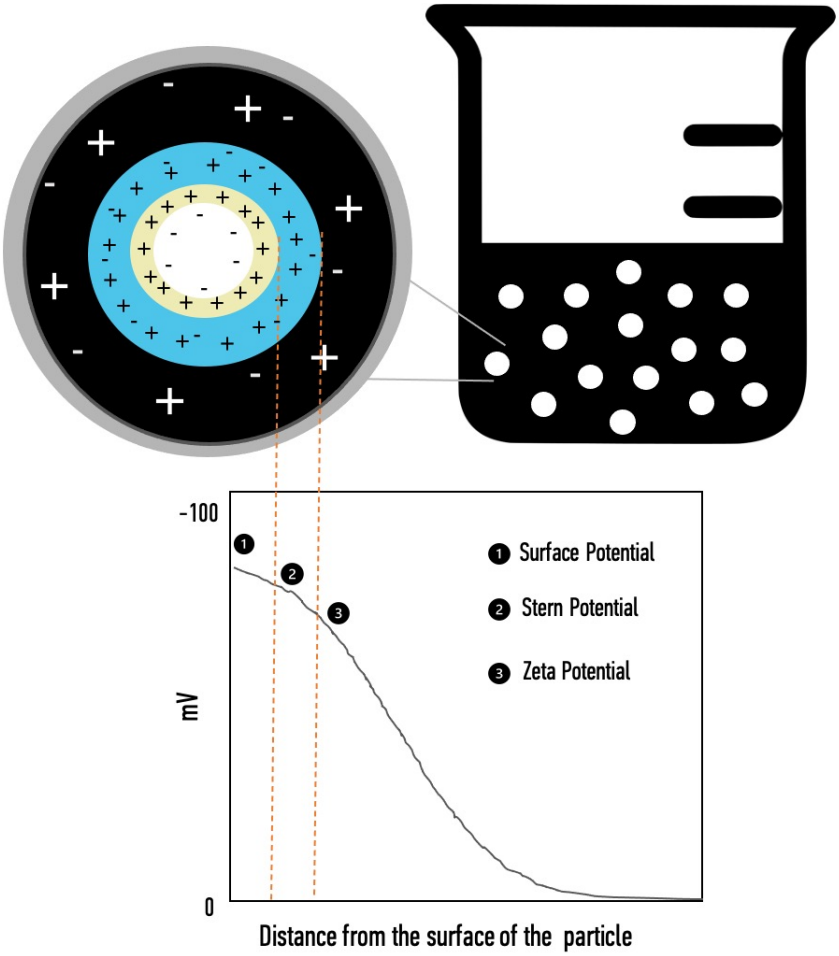

Figure 1 Illustration of the electric double layer, Stern potential, diffuse potential, and Zeta potential

1.5. Rheological Behaviors of Non-Newtonian Liquids

Non-Newtonian fluids do not exhibit a linear relationship between shear rate and shear stress [1, 14]. Viscosity, which is the slope of the shear stress vs. shear rate graph, is not constant thereof. Many materials that do not have liquid-like consistency fall under this category. Some examples are; concrete, pastes, reinforced polymer melts [15–19].

Two of the most common non-Newtonian behaviors are shear thinning and shear thickening, which are nonlinear viscoelastic flow behaviors [1, 14, 20]. The viscosity decreases with the shear rate in shear-thinning materials, whereas it increases as a function of shear rate in shear thickening materials. The response that the material exhibits can be either intrinsic or can be modified between these two behaviors depending on many factors such as the particle size, surface properties, and suspension stability. The

structural rearrangement of shear-thinning is ordered by the breaking of the weak bonds in particle clusters at high shear rates. In shear thickening, the structure is disordered when individual particles form colonies, which is governed by hydrodynamic lubrication [20].

Another important concept is the thixotropy. It is defined as the continuous decrease of viscosity with time when shear is increased, which is reversible upon the arrest or decrease of shear. This phenomenon implies time and shear history dependency, as if the microstructure of the material has a "memory" that can be recovered, creating a hysteresis loop thereof [21].

1.6. References

[1] T. G. Mezger, *The Rheology Handbook*, 4th ed., vol. 59, no. 4. Hanover: Vincentz Network, 2014.

[2] S. Cinar, "Rheological behavior of oxide nanopowder suspensions," Iowa State University, 2013.

[3] C. F. Ferraris and J. M. Gaidis, "Connection between the rheology of concrete and rheology of cement paste," *ACI Mater. J.*, 1992.

[4] M. Jabbari, R. Bulatova, A. I. Y. Tok, C. R. H. Bahl, E. Mitsoulis, and J. H. Hattel, "Ceramic tape casting: A review of current methods and trends with emphasis on rheological behaviour and flow analysis," *Materials Science and Engineering B: Solid-State Materials for Advanced Technology*. 2016.

[5] M. E. Mackay, "The importance of rheological behavior in the additive manufacturing technique material extrusion," *J. Rheol. (N. Y. N. Y).*, vol. 62, no. 6, pp. 1549–1561, 2018.

[6] C. Shi, Z. Wu, K. Lv, and L. Wu, "A review on mixture design methods for self-compacting concrete," *Constr. Build. Mater.*, vol. 84, pp. 387–398, 2015.

[7] K. Prabhakaran, A. Melkeri, N. M. Gokhale, T. K. Chongdar, and S. C. Sharma, "Direct coagulation casting of YSZ powder suspensions using MgO as coagulating agent," *Ceram. Int.*, vol. 43, no. 1, pp. 316–323, 2009.

[8] H. A. Barnes, "Rheology of emulsions - a review," *Colloids Surfaces A Physicochem. Eng. Asp.*, vol. 91, pp. 89–95, 1994.

[9] T. Tridib and D. Bhudeb R., "Flocculation : A New Way to Treat the Waste Water," *J. Phys. Sci.*, vol. 10, pp. 93–127, 2006.

[10] R. Hogg, “Bridging flocculation by polymers,” *KONA Powder and Particle Journal*. 2012.

[11] T. Tadros, “Electrostatic and Steric Stabilization of Colloidal Dispersions,” in *Electrical Phenomena at Interfaces and Biointerfaces: Fundamentals and Applications in Nano-, Bio-, and Environmental Sciences*, 1st ed., H. Ohshima, Ed. John Wiely & Sons Inc., 2012, pp. 1–20.

[12] J. D. Clogston and A. K. Patri, “Zeta potential measurement.,” in *Methods in molecular biology (Clifton, N.J.)*, Springer Science+Business Media, 2011, pp. 63–70.

[13] A. R. Studart, E. Amstad, and L. J. Gauckler, “Colloidal stabilization of nanoparticles in concentrated suspensions,” *Langmuir*, vol. 23, pp. 1081–1090, 2007.

[14] A. Y. Malkin and A. Isayev, *Rheology. Concepts, Methods, and Applications: Concepts, Methods, and Applications: 3rd Edition*. Toronto: ChemTec Publishing, 2017.

[15] Z. Yilmaz, M. Dogan, and M. Alkan, “Rheological and wall slip properties of kaolinite-silicon oil pastes during extrusion,” *J. Ceram. Process. Res.*, 2010.

[16] P. F. G. Banfill, *Rheology of Fresh Cement and Concrete*, 1st ed. London: CRC Press, 1991.

[17] Y. Y. Zhang and S. X. Wang, “Rheological and flocculated properties of silver nanoparticles paste,” in *Advanced Materials Research*, 2011.

[18] R. Shaughnessy and P. E. Clark, “The rheological behavior of fresh cement pastes,” *Cem. Concr. Res.*, 1988.

[19] M. R. Kamal, L. A. Utracki, and A. Mirzadeh, “Rheology of polymer alloys and blends,” in *Polymer Blends Handbook*, 2014.

[20] J. M. Brader, “Nonlinear rheology of colloidal dispersions,” *Journal of Physics Condensed Matter*. 2010.

[21] J. Mewis and N. J. Wagner, “Thixotropy,” *Adv. Colloid Interface Sci.*, vol. 147, pp. 214–227, 2009.

CHAPTER 2

FORMULATION OF PRINTABLE HIGH-STRENGTH LIGHTWEIGHT CEMENT-BASED MATERIALS

2.1. Introduction

One of the Additive Manufacturing (AM) techniques, known as the layer-by-layer deposition, in cement-based systems has pioneered numerous studies to investigate the fresh properties of cementitious materials [1–8]. Using a printer on construction sites boosts the process efficiency by minimizing the overall cost and duration of a project, as well as the risk of on-site fatal accidents of laborers [9]. Concerning various architectural demands, having control over the deposited material —without the need to use expensive formwork— enables the deposition of complex geometrical designs [6, 10]. Furthermore, the automated nature of the process enables the use of cement-based materials in spatial applications [11].

Similar to the successful AM models followed for various materials in disciplines outside of the construction field, not only the specifications of the printer (model, motor capacity, nozzle size) are considered to be the governing parameters, but also the material formulation [12–14]. Current formulations of ordinary Portland cement (OPC), silica fume, quartz, metakaolin, kaolin, and limestone filler with 1–3% of additives are used and optimized to obtain stable and buildable cement-based filaments [15]. However, these formulations principally targeted OPC-based cementitious systems due to the lack of commercially available rheology-modifying additives (RMA) or high range water reducers (HRWR) for other types of cement-based materials. As 3D-printing applications heavily depend on the rheology of the medium, the lack of an RMA compatible with the particles means not reaping the benefits of the properties of the material coming from i) other types of cement such as white cement and ii) an increase in the content percentage of waste materials [16–18]. Consequently, systems containing only OPC and a low

percentage of other cementitious materials resulted in high strength, low density, or high thermal resistance but lacked the inclusivity of all of the three features together [19].

Therefore, to prepare a formulation that results in all of the three features, there is a need for an RMA that can cater to controlling all of the added particles [20, 21]. In this thesis, an AMPS-modified poly(carboxylate ether)-based RMA was produced and tested with white cement and two new types of recycled waste materials, silica fume, and cenosphere particles. This grafted polymer was found to be compatible with other cementitious particles, including OPC, limestone, clay, and gypsum [22]. To achieve the desired thixotropic behavior of the cement paste, two mechanisms were introduced in the system: electrostatic repulsion and steric hindrance. Such an active control of the rheology of the fresh state enabled the system to be extrudable and buildable. Moreover, it facilitated the use of fewer amounts of water, which contributed to higher early-strength values of the mixture in its hardened state.

To successfully extrude stable cementitious filaments, we studied the electrokinetic behavior of the particles and the rheological behavior of the paste in its fresh state. To ensure high-performance requirements, we measured the compressive strength and the dry hardened density of the mortar and performed a thermal analysis on a matrix of mixtures in their hardened state. Our best-performing mixture results in a high-strength of 80 MPa reachable after 28 days, an 11% reduction in the dry hardened density, and a thermal resistance (insulation) of 0.63 mK/W. According to ACI, this formulation is classified as high performance (>55 MPa) and lightweight (320–1920 kg/m^3).

Overall, we explored the influence of using the designed RMA on the properties of high-performance cement-based materials by i) proposing the use of white cement for its rapid high-strength gain and ii) replacing relatively high percentages of the cement content by silica fume and cenosphere particles. These waste materials were selected as the former contributes to the compressive strength and the latter results in an increase in the thermal resistivity and a decrease in the overall weight of the hardened product. Finally, this work acknowledges that the properties of the selected cementitious materials, as well as the additives, govern the behavior of extrudable formulations and can significantly enhance or diminish the quality of the final deposited layers.

2.2. Materials & Sample Preparation

2.2.1. Materials

To prepare the RMA as a polymer solution, the following chemicals, whose molar masses are given in Table 2.2.1, were used. Acrylic Acid (AA, 99%), 2-Acrylamido-2-Methylpropane Sulfonic Acid (AMPS, 99%), Potassium Persulfate (KPS, ≥ 99%), and Hydrochloric Acid (HCl, 37%) were acquired from Sigma Aldrich. Polyethylene Glycol (PEG), Sodium Hydroxide (NaOH, ≥ 97%), and Maleic Anhydride (MA, 99%), were purchased from Merck. Deionized water was used throughout all of the experiments.

Table 2.2.1 Molar masses of the chemicals used in the polymer synthesis (g/mol):

AMPS	207.0
AA	72.06
PEG	1000
NaOH	40.00
MA	98.06
KPS	270.3

Throughout all the testing of the cement-based mixtures, the samples were prepared using the following materials: white cement that complies with BS EN 197-1:2012 from Çimsa, a local cement producer in Turkey [23]. Cenosphere particles (Ceno) LS300 were sent by New York University Abu Dhabi, United Emirates. Silica fume (SF) was purchased from DOSTKIMYA, Turkey. CEN standard sand was purchased from UTEST in Turkey.

Table 2.2.2. Cementitious particles properties

Material	Cement	SF	Ceno	Sand
Density (g/cm^3)	3.06	0.25–0.35	0.32–0.44	2.64
The diameter of the particle (mm)	1	$< 10^{-3}$	10^{-3}–1.00	0.08–2.00
BET surface area (m^2/g)	1.65	15–28	2.50–4.57	-

2.2.2. Synthesis of the Grafted Copolymer (RMA)

The RMA is designed as a grafted AMPS-PCE copolymer wherein the monomers are AMPS, AA, and PEG. Thus, to obtain an aqueous solution containing 12–15 wt. % solid content of the grafted copolymer, the procedure was carried out according to Salami and Plank [24]. This model was chosen as it has been successfully proven to be effective in terms of dispersing cementitious and ceramics particles by Akhlaghi et al. [22, 25]. Firstly, to enable the polymerization of PEG with AA, PEG was esterified with MA according to the esterification procedure described by Lu et al [26]. Thus, the esterified product, PEGMA was used thereafter, without further purifications. The free-radical polymerization process began with preparing (any multiple of) a 110 ml solution in which PEGMA, AMPS, and AA were dissolved according to the desired molar feed ratios. Table 2.2.3 shows the ratios that were selected for the rheological testing; the pH level of all the solutions was kept at 8 using aqueous solutions of NaOH and HCl [22]. Following the pH adjustment, the solution was charged into two-neck or three-neck flasks that have a capacity of 300–500 ml, which were then connected to the reflux condensers. While waiting for the temperature to reach 50 ˚C, nitrogen gas was purged to remove any free oxygen for 30 min. Meanwhile, two doses of the initiator of 0.25 g KPS in 10 ml aqueous solution each (for a 110 ml solution) were prepared. At 50 ˚C, the first dose of the initiator was added, and the temperature was then raised to 60 ˚C for 50 minutes. At 60 ˚C, the second dose was added for 75 minutes and then the temperature was increased to 80 ˚C for 5 hours. At the end, the reaction is turned off and cooled down to room temperature (22 ˚C). The final product of any of the grafted copolymer solutions was either left as an

aqueous solution[2] or precipitated to obtain a solid form of the polymer. The precipitation process was done in alcohol and the precipitates were left to dry at 50 ˚C overnight under a vacuum.

Table 2.2.3. The molar feed ratio of the grafted copolymer

Grafted Copolymer acronym	**Molar feed ratio (AMPS/AA/PEGMA)**
A25-P0.33	25:25:0.33
A25-P0.11	25:25:0.11
A25-P1	25:25:1
A25-P1.66	25:25:1.66
A25-P2	25:25:2
A25-P5	25:25:5

2.2.3. Samples Mixture Proportions

The overall materials proportions are presented in Table 2.2.4. For rheology measurements, cement paste samples were prepared with water-to-binder (w/b) ratios of 0.26 and 0.38, an amount of 50 g of cementitious materials was sufficient for these experiments. For the rest of the tests that were carried out on the cement-based mixtures, mortar[3] samples were prepared with a water-to-binder ratio of 0.38 and 400 g of cementitious materials were used. Additionally, to investigate the performance of utilizing the recycled materials —SF and FACs, a control mixture of only cement, sand, and w/b of 0.38 was prepared. The w/b was fixed at 0.38 because it is the minimum value required to achieve full cement hydration. Any value less than 0.38 would require extra curing processes of the hardened product to gain adequate compressive strength [27].

[2] When the grafted copolymer solution was used in further testing, the extra water was subtracted and the added amount was calculated based on the solid content of the solution, which was measured using the moisture analyzer by Shimadzu, uniBloc MOC63u.

[3] Mortar = cement paste + sand

Table 2.2.4. Cement-based mixtures proportions

FAC	0%, 10%, 15%, 20%, 25%, 30% & 50%
SF	8%
Cement	(100-FAC-SF) %
Cement to sand	1:2.25
w/b	0.26, 0.38
RMA	1.5%

2.2.4. Samples Mixture Procedure

Inspired by the ASTM standards (ASTM C 305 – 06) and EN standards (BS EN 196-1) for mechanical mixing of hydraulic cement pastes and mortars, a modified mixture procedure was optimized [28, 29]. For the cement paste, Heidolph RZR 2102 with a 4-bladed propeller mixer was utilized with the succeeding steps:

1. The cementitious materials were mixed until homogenized while dry for 10 seconds.
2. The powder was added to the water and mixed at slow speed (140 ± 5 rad/min) for 30 seconds.
3. The mixture was paused for 10 seconds and the sides were scraped down.
4. Lastly, it was mixed at high speed (280 ± 5 rad/min) for 90 seconds.

For the mortar, Hobart mixer was used with the succeeding steps:

1. The cementitious materials were mixed until homogenized while dry for 20 seconds.
2. The powder was added to the water and mixed at slow speed (65 rpm) for 30 seconds.
3. The sides were scraped down to remove any excess powder and the sand was added.
4. Again, the mixture was mixed at slow speed (65 rpm) for 30 seconds.
5. Again, the sides were scraped down to make sure the mix was homogeneous, and no excess powder is left.
6. Lastly, it was mixed at high speed (125 rpm) for 90 seconds.

2.2.5. Samples Molding and Curing

The molding and curing conditions were set up according to EN 196-1; nine 40mm × 40mm × 40mm cubic molds were used [29]. The molds were oiled and filled in 3 layers and the mortar was tampered 25 times at every layer. The surface was smoothed off and covered with a damp cloth and a plastic membrane to lock the surface moisture for the first 24 hours. After one day from the initial time of molding, the mortar cubes were de-molded and placed in a water tank at a sufficient submerging depth. The tank was filled with deionized water that was kept at a temperature range of 23–26 ˚C (± 1 ˚C due to the ambient conditions of the laboratory), until the testing day for compressive strength and dry hardened density—7 days and 28 days later. To conduct the thermal analysis on the mortar cubes, the same molding and curing procedure is followed except that the size of the cubes was 50×50×50 mm^3 because testing on larger samples results in more accurate measurements [30].

2.3. Experiments & Testing

2.3.1. Electrokinetic Characterization

The white cement, cenosphere and silica fume suspensions were prepared with w/b = 40 and 0–1.5 wt. % RMA. This high w/b ratio was selected to remove the background noise in zeta potential measurements, whereas both a high and a low w/b ratio are comparable (refs from CAC paper). The suspension was then diluted with deionized water at 1/5 vol/vol to keep the conductivity of the medium at 18 mS/cm [31]. The suspensions were mixed magnetically for 10 min, sonicated for 3 min, and mixed magnetically for 3 min again. Then, to study the electrokinetic behavior of these samples, their zeta potential and its values in the presence of various amounts of the added RMA was tracked by employing the device called Zetasizer nanoseries, Malvern Instruments with a red laser of 633 nm. The device reported the results of 6 measurements that were run at least 12 cycles each at 25 ± 1 ˚C. Each measurement was taken based on the Smoluchowski approximation, in which the electrophoretic mobility of particles is determined [32].

2.3.2. Rheological Characterization of the Cement Paste

Following the mixture procedure for the cement paste, while it is still in its fresh state, its flowability was assessed using the rheometer Anton-Paar MCR302. This device operates at 25 ± 1 ˚C and is equipped with a parallel plate of 25 mm in diameter. The gap size between the plate and the sample was set to 1 mm for all measurements. Loaded immediately upon starting, initially, the device measures the viscosity of the sample with a constant shear rate of 100 s^{-1} for 20 seconds. Then it is measured by gradually decreasing the shear rate until 1 s^{-1} for 13 seconds followed by more measurements with increased shear rate from 1 s^{-1} to 100 s^{-1} again for 13 seconds. The acquired data is then plotted on a viscosity (Pa.s) versus the increasing and decreasing shear rate (s^{-1}) graph to investigate the shear-thinning behavior of the mixtures with the additive.

2.3.3. Characterization of Fresh Properties

To assess the dispersibility of the RMA on the cement paste the conventional mini-slump test developed by Khayat and Yahaya was performed [33]. The Neat cement paste and FAC20 paste samples were prepared at w/b = 0.38 with varying added weight percentage of the additive and mixed as described in 2.2.4. A cone with 60 mm height, 20 mm top diameter, 40 mm bottom diameter was utilized during the test. The cone was placed on a sheet of plexiglass at a leveled surface at 22 ± 2 ˚C and filled with the paste. Immediately after that, the cone is lifted, and the spread of the paste is recorded in two perpendicular directions. The average of the two spread diameters was then reported as the final result. For further investigation of the mortar samples, which included sand as another particle in the cementitious system, the same test was performed again. The mixture was placed inside the cone following BS EN 1015-3, in 3 portions each tampered 25 times [34]. In this case, instead of the slump diameter, the slump loss with respect to the flipped cone height was recorded.

2.3.4. Characterization of Hardened Properties of the Mortar

2.3.4.1.Compressive strength

Six out of the nine cubes that were removed from the water tank after 7 days and 28 days were tested for their compressive strength. According to EN 196-1:1995, the compressive strength was recorded using a Cement-Mortar compression machine 250 kN, Cyber-plus evolution MATEST (Model: E159-01N) with two squared grips to match the size of the cubes [29]. The machine applies stress at 2.400 MPa/sec with a starting load of 5 kN and a maximum load of 250 kN. It then automatically displays the individual ultimate stress of the cubes by dividing the maximum force they can withstand with the cross-sectional area, which is constant for all of them and is equal to 1600 mm^2. Then the average value of the stresses was calculated and reported as the final result of the compressive strength for each mixture.

2.3.4.2.Dry Hardened Density

Following BS EN 1005-10:1999, the other 3 cubes were dried in a BINDER-Series VD (Model: VD 115) oven at 105 ˚C [35]. After letting the cubes dry overnight, their dry mass was measured the next day multiple times until two consecutive measurements – measured two hours apart– do not differ by more than 0.2%. Then, by dividing the dry mass $M_{s,dry}$ to the volume of the cube V_s, which is equivalent to the volume of one cubic mold, the density was calculated as $\rho_s = \frac{M_{s,dry}}{V_s}$ and reported in kg/m^3.

2.3.5. Thermal Analysis of the Mortar

Complying with the EN standards BS EN 12664:2001, the cubes were tested under dry conditions —28 days later after curing plus 1 day of drying off the moisture, which was done according to the procedure described in BS EN 1015-10 [35, 36]. Also, with the respect to the models proposed by the standards, the instrument Hot Disk TPS 2500 S was employed to perform the thermal analysis on these mortar cubes [37]. The way this device operates is that a sensor, which is made of a spiral of electrically conducting material (nickel foil), is sandwiched between two thin sheets of an insulating material such as Kapton or mica. The sensor is then put between two identical samples —in this case, mortar cubes of 50×50×50 mm^3. After adjusting the samples in the desired condition, in this case, dry conditions at both T = 25 ˚C and T = 45 ˚C, an electrical

current is run to increase the temperature of the sensor. At the same time, the analyzer instrument (TPS2500) monitors the increase in resistance as a function of time following the transient plane method. Each experiment was run 5 times and recorded, then the average value of the thermal conductivity was reported.

2.4. Results & Discussion

2.4.1. Colloidal Study of the Particles with the Grafted Copolymer

2.4.1.1.Rheology-controlling mechanism

The chemical structure of the synthesized grafted copolymers is depicted in Figure 2. The backbone of the polymer is made up of AMPS and AA, and the side chain of the polymer is PEGMA. The polymer overall has a negative charge; AMPS primarily contributes to the negativity as it belongs to the sulfonate group which has 3 oxygens. AA only partially contributes to the negativity with its OH– end functional, however, PEGMA does not contribute to the charge as it is neutral.

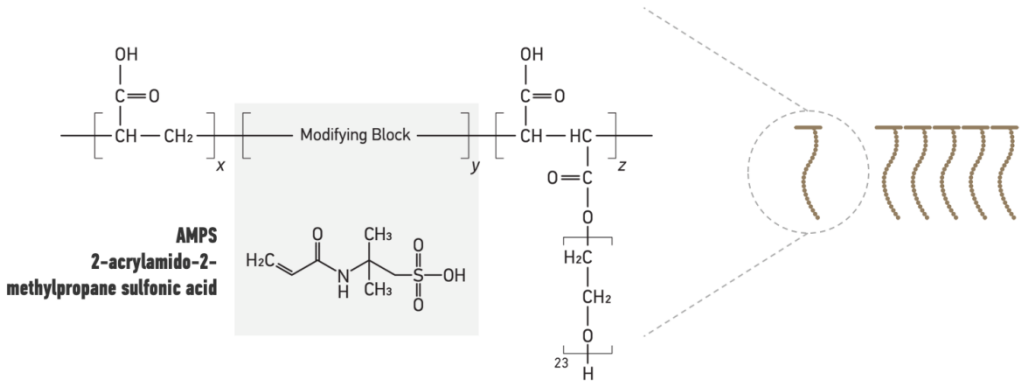

Figure 2 Chemical structure of the grafted copolymers

As demonstrated in Figure 3, when the grafted copolymer is added to the cement suspension, it is attracted to the positively charged cement particles and thus the negative backbone adsorbs onto the particle. The so coated particles will repel each other by what is called electrostatic repulsion [38]. Concurrently, the PEGMA side chain extends in the aqueous medium due to its hydrophilic features, thus, creating an extra buffering layer between the particles, this mechanism is referred to as steric hindrance [39].

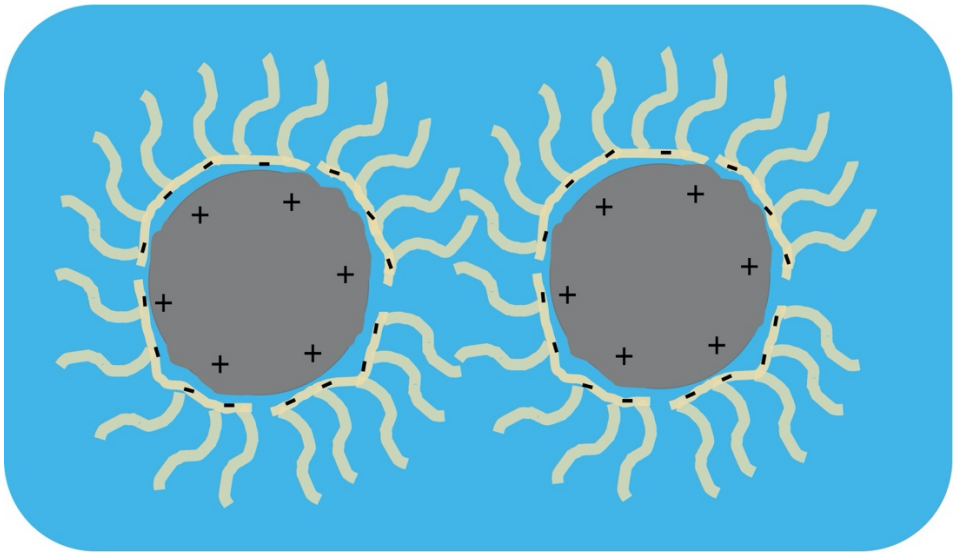

Figure 3 Electrostatic repulsion and steric hindrance mechanism of the grafted copolymer with the cement particles below 1.5 wt. %

2.4.1.2.Electrokinetics and adsorption behavior of the RMA with particles

Owing to the negativity of the monomers AMPS and AA, the predominant charge of the grafted copolymer was negative [22]. Thus, to further evaluate the rheology-modifying ability of the negatively charged additive P1 with each of the particles, their zeta potential (ZP) at different dosages was tracked, as shown in Figure 1.

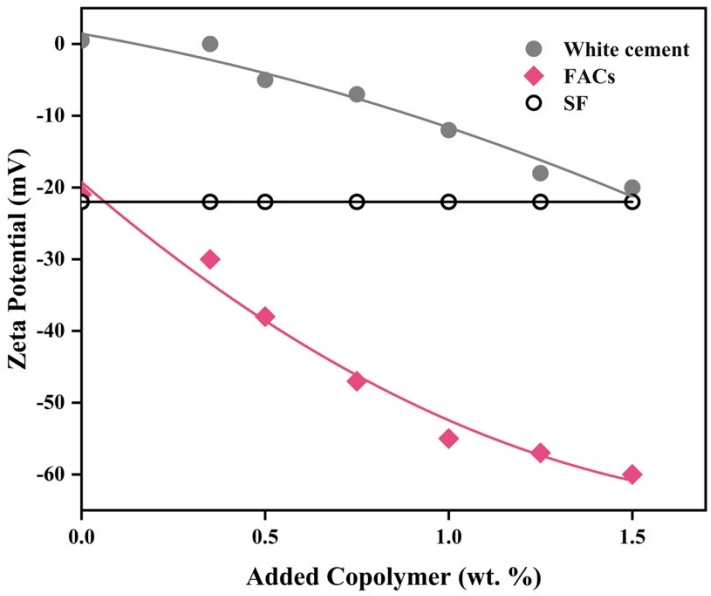

Figure 4 Zeta potential of cement, cenosphere, and silica fume in the presence of various percentages of P1

The neat ZP of white cement was close to zero, and the particle was assumed to have a positive surface charge. With increased wt. % of the added copolymer, the ZP of the white cement suspension was brought to –20 mV, which corresponds to the minimum ZP absolute value required to reach a stable suspension. The neat ZP of FACs started at –20 mV, thus the particles had a negative surface charge. When the copolymer adsorbed onto the FACs particles, it maximized the negativity of the suspension, reaching –60 mV at 1.5 wt. %, which is indicative of a highly stable colloid. The neat ZP value of silica fume was -21 mV and it stayed constant in the presence of the polymer. This indicated that there was no chemical bonding, through functional groups, between the particles and the additive [22, 25]. This electrokinetic study signifies that the working mechanism of the grafted copolymer (section 2.4.1.1), increased the stability of the suspended particles, mainly FACs and white cement, at 1.5 wt. %, which in turn decreased the agglomeration.

2.4.2. Rheological Characterization of the Cement Paste

To understand the influence of the RMA on the rheological behavior of the neat white cement paste, two samples control and with added RMA were compared at increasing and decreasing shear rates. Viscosity wise, Figure 5 depicts the modified fluidizing behavior of the cement paste that is gained upon the addition of the RMA, which can be attributed to the rheology-controlling mechanism explained in section 2.4.1.1. The minimum RMA value of 0.5 wt. % was sufficient to achieve a fluidizing effect in the paste, further addition of the additive flowed similarly.

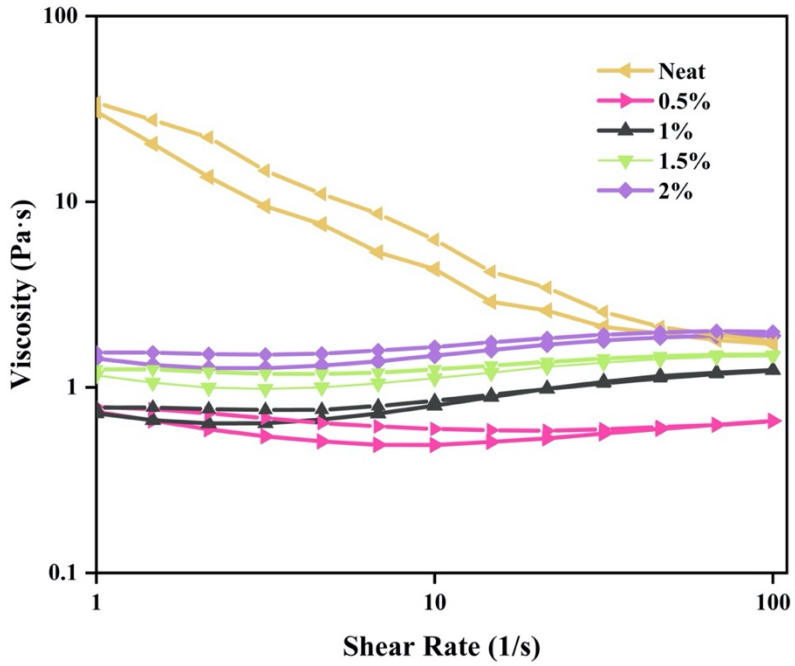

Figure 5 Viscosity as a function of the shear rate of the white cement paste in the presence of different amounts of P1, displaying thixotropic behavior

Shear stress-wise, Figure 6 confirms the fluidizing nature of the pastes in the presence of the RMA as the response the material displays is like a Newtonian fluid. Newtonian fluids are characterized by having no yield stress; therefore, the shear stress curve intercepts the x-axis at the origin. The curves containing any percentage of the RMA start from zero. In contrast to the neat sample that exhibited a non-Newtonian response, especially for a shear rate in the range of 0–40. The yield stress, in this case, is non-zero since the curve starts at approximately 25 Pa.

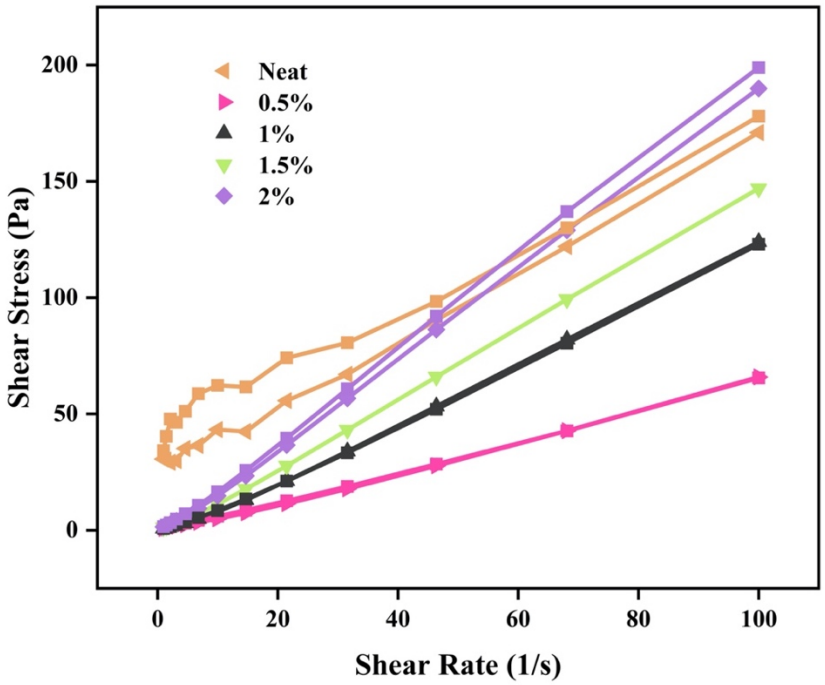

Figure 6 Shear Stress as a function of the shear rate of the white cement paste in the presence of different amounts of P1, displaying thixotropic behavior

The introduction of the RMA to the system was anticipated to result in an ordered distribution of the particles as well as decreased agglomeration. Therefore, to evaluate the behavior of the RMA at 1.5 wt. % and confirm its compatibility with all the particles, the viscosities were measured for each 50 wt. % suspension separately and compared with the neat samples (Figure 7). At shear rate 1 s^{-1}, the RMA decreased the viscosity of the silica fume suspension by 90%. While the viscosity of the FAC suspension was increased by 85%, this increase can be due to its high concentration. Moreover, the addition of the RMA decreased the white cement paste viscosity was about 97%. At shear rate 10 s^{-1}, all the suspensions converged to the same viscosity value around 1 Pa.s, in the presence of 1.5 wt. % RMA. However, the behavior over the entire range of each of the particles was different. Silica fume displayed a shear-thinning behavior, FAC and white cement displayed a rather Newtonian fluid behavior.

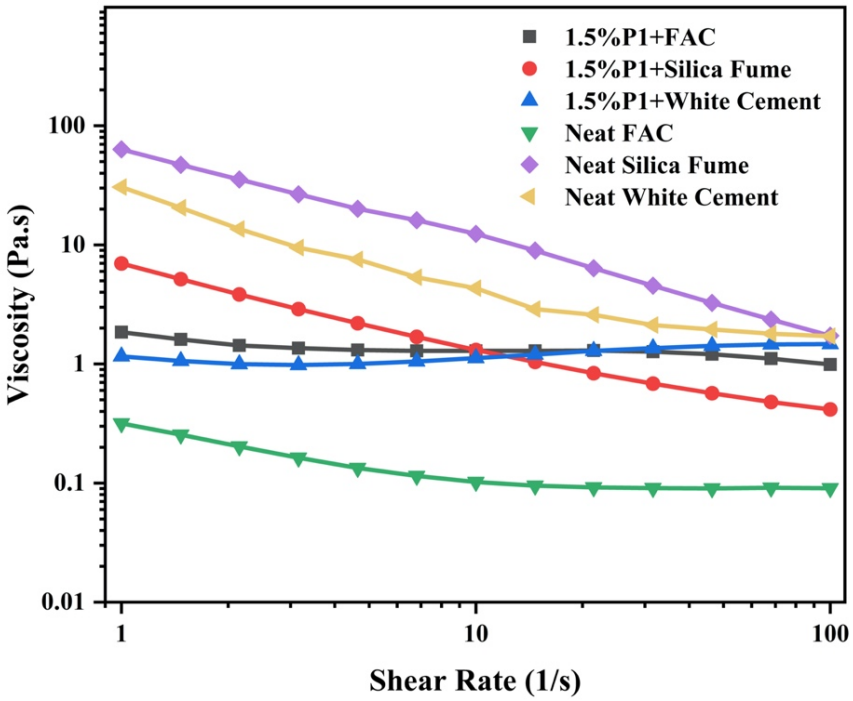

Figure 7 Effect of 1.5 wt. % RMA on each of the particles separately on suspensions with 50 wt. % particle-loadings

To optimize the additive in terms of the molar feed ratio of the monomer PEG1000 that comprises the side chain, we traced its effect on shear viscosity in the range of 0.11–5 molar feed ratio of PEG/(AMPS + AA). Being the only varying monomer, the names are indicative of this molar feed ratio. Notwithstanding the effect of water, we kept the w/b ratio at 0.26 and chose a mid-value of SCMs amount of 28% for this analysis. As for the characteristics of the backbone, the molar feed ratio of the monomers AMPS/AA to each other was constant at 1, based on the positive results obtained in our previous work [22]. All the curves in Figure 8 demonstrate a decreasing trend with the increased shear rate; therefore, the overall behavior of the paste was shear thinning. Moreover, the viscosity at each shear rate of the pastes decreased up to molar feed ratio 1 and increased again beyond that with additives P2 and P5, indicating that P1 is the optimum additive. This behavior can be explained by the steric hindrance action among the particles that is induced by the PEG1000 side chain, which is attributed to its hydrophilicity, when the side chain got larger with higher molar feed ratios, the chains can intertwine causing an increase in the viscosity thereof [39, 40].

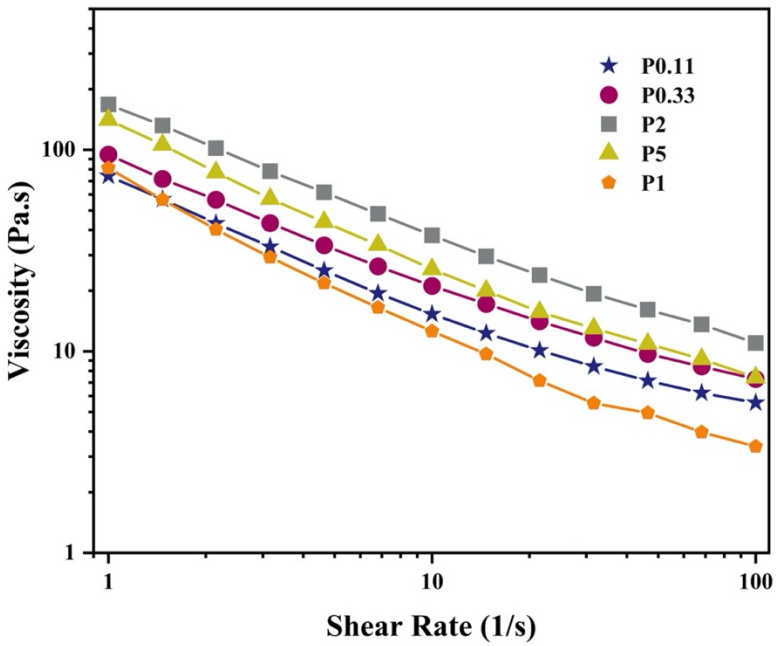

Figure 8 Effect of the side chain density on the rheology of FAC-20 paste at w/b = 0.26 in the presence of 1.5 wt. % of each of the grafted copolymers

Moreover, to investigate the performance of the additive with different FACs content in the presence of P1, the viscosity of pastes at a w/b ratio of 0.38 and 8% silica fume were evaluated. Here, we increased the w/b ratio to account for the true behavior that the paste will exhibit later upon the addition of the standard sand.

Firstly, compared with the curves in Figure 7, the predominant behavior in Figure 9 was shear thinning. As given in Table 2.2.2, the surface area of the silica fume was much higher compared with the other particles, which is why it governed the behavior of the mixture. As shown in Figure 9, the curve FAC-30 reached the minimum viscosity at lower shear rates indicating an optimum SCMs amount up to 38%, which increased the workability of the paste. However, beyond that point, more FACs content had an adverse effect on the workability, as is depicted in the figure, the FAC-50 curve was approximately 2 orders higher than the FAC-0 and CM pastes. At lower shear rates, we reasoned that the workability increases because the FAC particles are spherical in shape and larger in size compared to the cement particle [41]. Nonetheless, after a FACs replacement of 30%, the decrease in workability can be the consequence of the packing of the particles at a high concentration [42].

At higher shear rates, the decay in viscosity in all curves can be linked to the release of water that occurs among particles in agglomerates. This mechanism is due to the shear-thinning phenomenon that is facilitated by the breakage of weakly-linked agglomerates [43–45]. This rheological study shows that the rheology-modifying additive was efficient in terms of changing the viscosity of the cement pastes containing silica fume and FACs, as well as increase the workability up to 38% SCMs

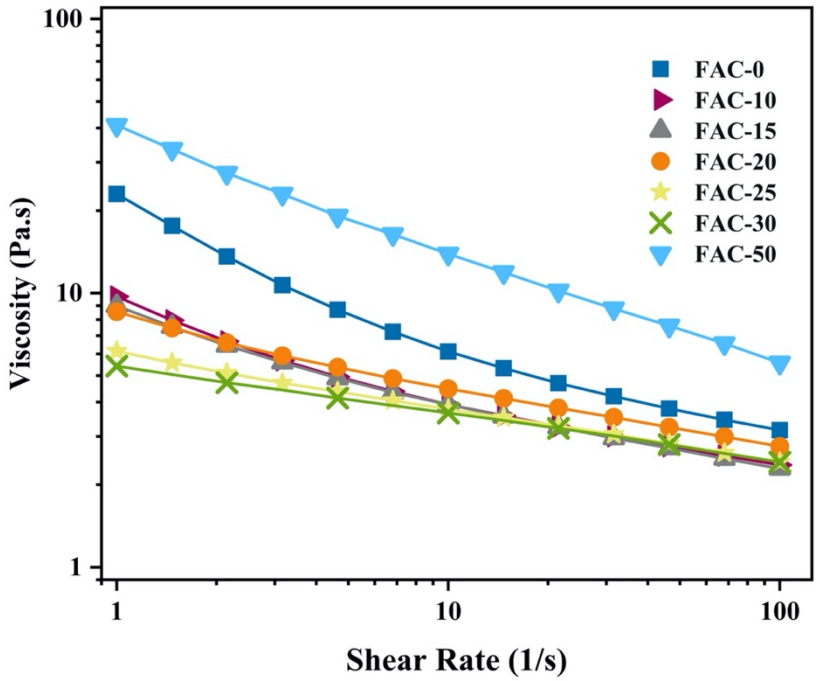

Figure 9 Effect of P1 at 1.5 wt. % on the rheology with varying FACs content at w/c = 0.38

2.4.3. Characterization of the Fresh Properties

To accompany the rheological characterization with a more conventional test of flowability, the mini-slump test was performed. The values given in Figure 10 validate the effectiveness of the RMA even at the low percentage of 0.5 wt. %, due to the fluidizing ability that is observed in Figure 6 as well. The spread diameter was increased by about 75% and 70% of the neat and FAC-20 samples, respectively. An RMA amount of 1.5 wt. % demonstrated the highest spread for both of the paste mixtures at approximately a 78% increase for the neat cement paste and a 72% increase for the FAC-20 paste. The difference in the slump flows within the two samples at 0 wt. % RMA can be attributed to the workability increase that the FAC content provides at 20%, which is observed in the difference of measured viscosities of the two samples in Figure 7 and Figure 8. For RMA values of > 0.5 wt. % both of the slumps level off equally, this demonstrates that when the particles are covered with the copolymer, their flow characteristics are similar, which is evident in Figure 8 as well. Observably, the paste is more homogeneous with a 1.5 wt. % compared to 0.5 wt. % as shown in Figure 11.

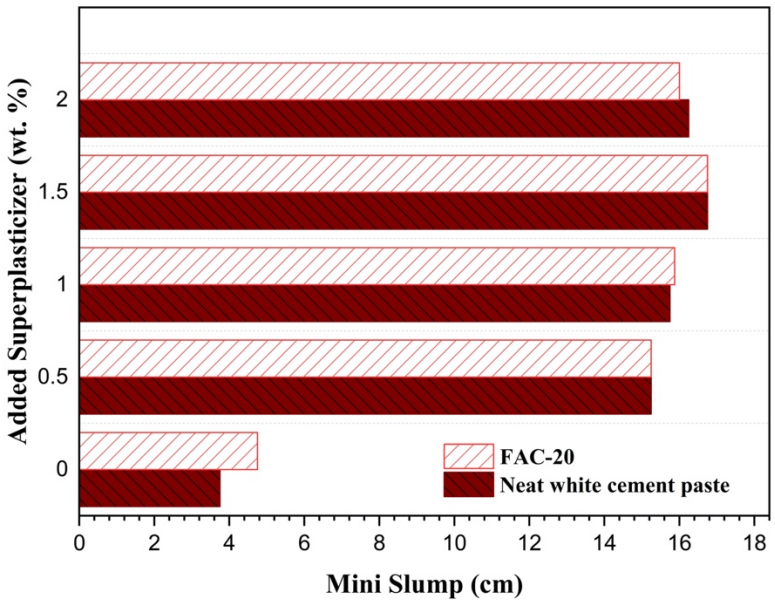

Figure 10 Average values of the mini-slump test on cement paste samples in the presence of different amounts of P1 polymer

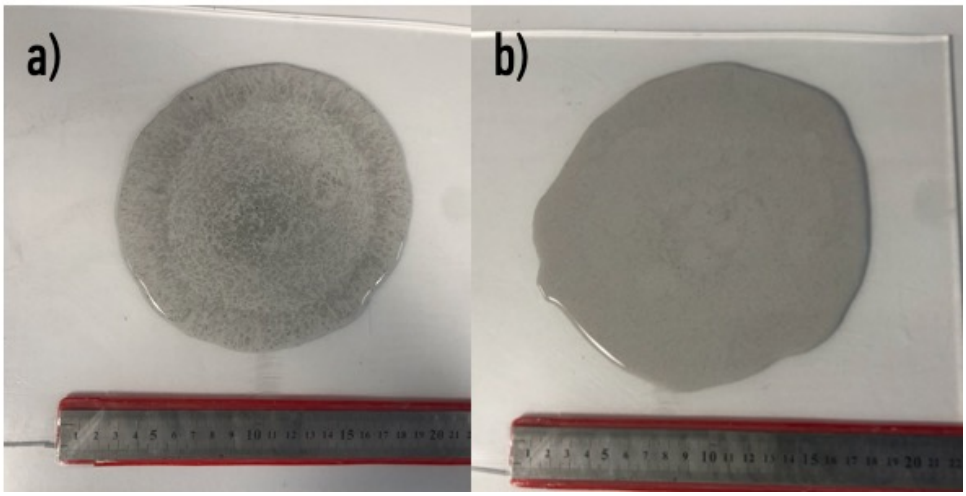

Figure 11 Spread of FAC-20 at a) 0.5 wt. %, and b) 1.5 wt. % addition of P1

The impact of standard sand addition into the cement paste was assessed with another set of measurements utilizing the mini-slump test for the height loss in comparison to the cone. Table 2.4.1 gives the values for mixtures with different FAC amounts. The neat sample that did not include any FACs demonstrated a 66.67% loss in height, as well as a minor spread, rendering the mixture unusable for extrusion. FAC-20 and FAC-30 mixture had, respectively, 1 cm (16.67%) and 0.5 cm (8.33%) loss in height. During the test, the material came out of the cone easily and this loss can be due to the release of pressure from the cone onto the material. This behavior showed promising results for the possibility of extrusion through a nozzle as the material was compact and did not shear after lifting the cone as illustrated in

Figure 12. In terms of workability requirements of extrudable cement-based systems, a slump of a value close to zero is indicative of an appropriate response to the extrusion [12]. On the other hand, the FAC-50 mixture displayed shearing in the material with respect to the slump, which is undesirable because it represents inhomogeneity and can lead to segregation and phase separation.

Table 2.4.1 Mini slump test results on mortar samples

Mortar Sample ID	Slump Loss (cm)	Comment
FAC-0	4	No shear, spread
FAC-20	1	No shear
FAC-30	0.5	No shear
FAC-50	-	Significant shear

Figure 12 Mini slump test on FAC-20 mortar sample with 1 cm loss in height

2.4.4. Characterization of the Hardened Properties of the Mortar

2.4.4.1. Compressive Strength

Figure 13 demonstrates the compressive strength that was conducted and evaluated at 7-day and 28-day ages. To assess the contribution of silica fume to the compressive strength of the system, we compared the two values between the control mixture (CM) and FAC-0. Both of the mixtures did not include any FACs amount, all variables held constant, the only difference in the formulation was the addition of 8% silica fume. This ratio was selected since adding higher values was proven to result in a decreased workability of the fresh mortar [46]. It was also the optimum value to maintain the loss of strength due to the addition of FACs. At 7-day age, FAC-0 was only 6% higher in strength, however, the effect of silica fume was more pronounced at 28-day age with a 10% increase —reaching the highest reported value at approximately 110 MPa. This late effect on strength occurs because silica fume induces a pozzolanic reaction in the system. Thus, it bonds with the calcium hydroxide (CH) product that results from the initial cement hydration forming new calcium silicon hydrate (CSH) products, which are responsible for the strength [47].

To investigate the effect of FACs as SCMs in the system, we studied the compressive strength of the mortar mixtures with varying contents of 0–50%. Expectedly, at a 7-day and 28-day age, the addition of more FACs in the system had a decreasing trend with the compressive strength values. Since FACs particles are hollow, they barely contribute to the strength, this impact intensified at high replacement

percentages [48, 49]. At 28-day age, for FAC-10, FAC-15, FAC-20, and FAC-25, the decrease was constant of about 8% for each 5% replacement, beyond that, at FAC-30, the decrease was steeper with about 16%. Nevertheless, all the mixtures up to FAC-30 at 28-day age were still classified as high strength (>55 MPa) despite the strength loss [50, 51]. At 7-day age, the decrease at each replacement was rather more random than constant, which we speculate is due to the delayed effect of silica fume. For FAC-50, the compressive strength significantly decreased, and the cubes were not physically durable. This behavior was realized as their failure under loading was due to having disintegrated rather than cracked and crushed. This type of failure and a large loss in strength is due to the presence of high FACs amount, and low white cement content. Whereas the silica fume donated only a small increase in compressive strength at 28-day age.

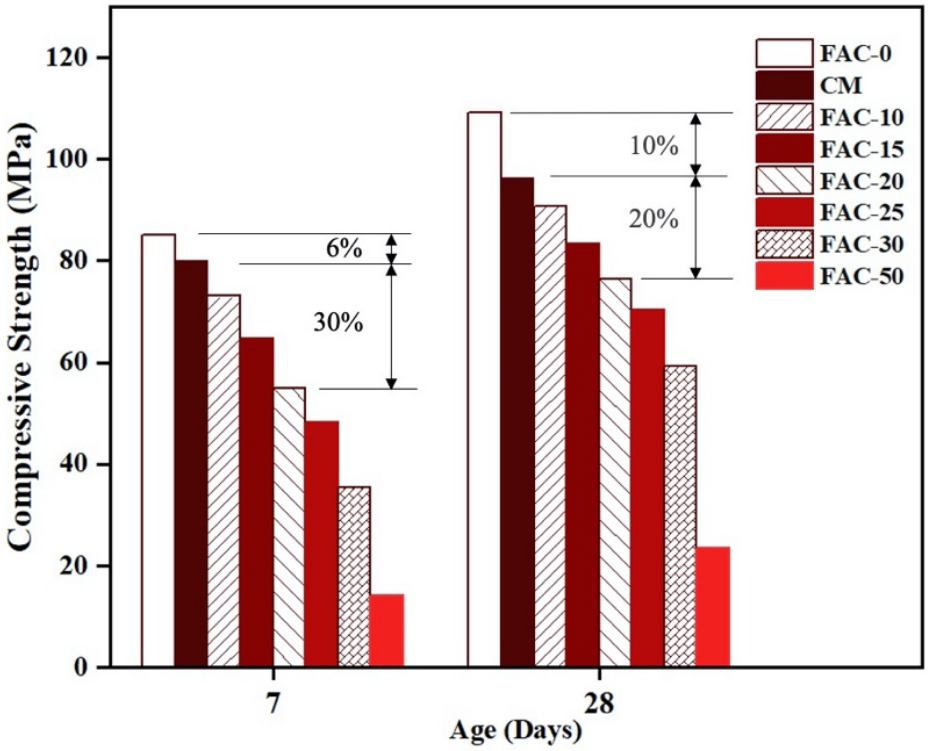

Figure 13 Compressive strength of the mortar mixtures after 7 and 28 days of curing in the presence of 1.5 wt. % RMA

2.4.4.2. Dry Hardened Density

According to ACI, conventional lightweight concrete has a maximum density of 1920 kg/m^3 [51]. Typically, lightweight cement-based materials have low compressive strength. In contrast, high-performance cement-based materials have densities of 2300–2500 kg/m^3 [52].

As can be seen in Figure 14, the CM and FAC-0 mixtures had approximately the same value of dry hardened density of a little over 2200 kg/m^3. Thus, there was no direct impact on the density from silica fume at 8% content. The general trend of dry hardened density was decreasing at a constant rate with the added amount of FACs. As they are hollow spherical particles of 300 microns, they had a much lower density of 0.32–0.44 g/cm^3. They also occupied more space than the other particles within the volume of the cube. Certainly, with this reasoning, the lightest set of cubes was FAC-50, with about a 32% drop from the density of both the CM and FAC-0. The mixtures FAC-20 and FAC-30, (38% resulted in 14% and 18% lower density compared to CM and FAC-0, respectively. The difference between the values of dry hardened density at 7-day and 28-day age was negligible.

Another crucial concept in lightweight structural cement-based materials is the specific strength, which is equivalent to the strength divided by the density [53]. The specific strength illustrates the trade-off between the strength and lightweight criteria, which makes it easier for engineers to choose the optimum mixture. Table 2.4.2 presents the values for each of the mixtures with different FACs amount. The use of SF increases the specific strength considerably in comparison to all the other values, on the other hand, the difference between FAC-20 and the CM mixtures was only 10%. Additionally, the cement-to-sand ratio was selected as 1:2.25 to keep the density minimized. According to Ban and Ramli who conducted an extensive study on the effect of the amount of added sand on the compressive strength, this ratio resulted in the highest strength [54].

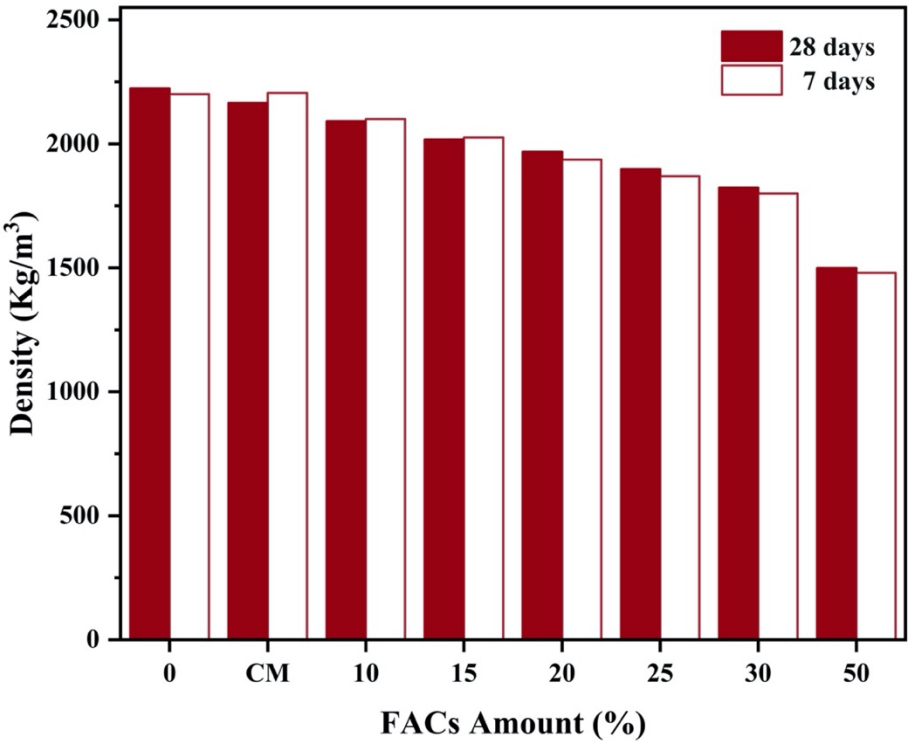

Figure 14. Density values with various FACs amount in mortar cubes in the presence of 1.5 wt. % RMA

Table 2.4.2 Specific strength of the cubes at 28-day age

FACs content	Specific Strength (kPa/kg m^{-3})
CM	43.56
0	49.10
10	43.41
15	41.34
20	38.82
25	37.10
30	32.48
50	15.65

2.4.5. Thermal Analysis of the Mortar

To realize the effect of FACs on the thermal properties of the cubes, the thermal conductivity was measured. The results are visible in Figure 15. The impact of silica fume on the thermal conductivity was studied by comparing the CM and FAC-0 mixture. An 8% SF content showed a mild contribution to the thermal insulation by a 1.3% decrease in thermal conductivity.

Matching our expectations for improved thermal insulation with more FAC particles in the system as they maximize the air content, the thermal conductivity had a decreasing trend [55], [56]. At both temperatures, the performance was almost identical for all the cubes; therefore, the effect of temperature from room temperature up to 45 ˚C was neglected. The FAC-50 mixture achieved the lowest thermal conductivity with about a 62% decrease from CM. As for the FAC-30 mixture, the thermal conductivity was 33% lower than that of the CM.

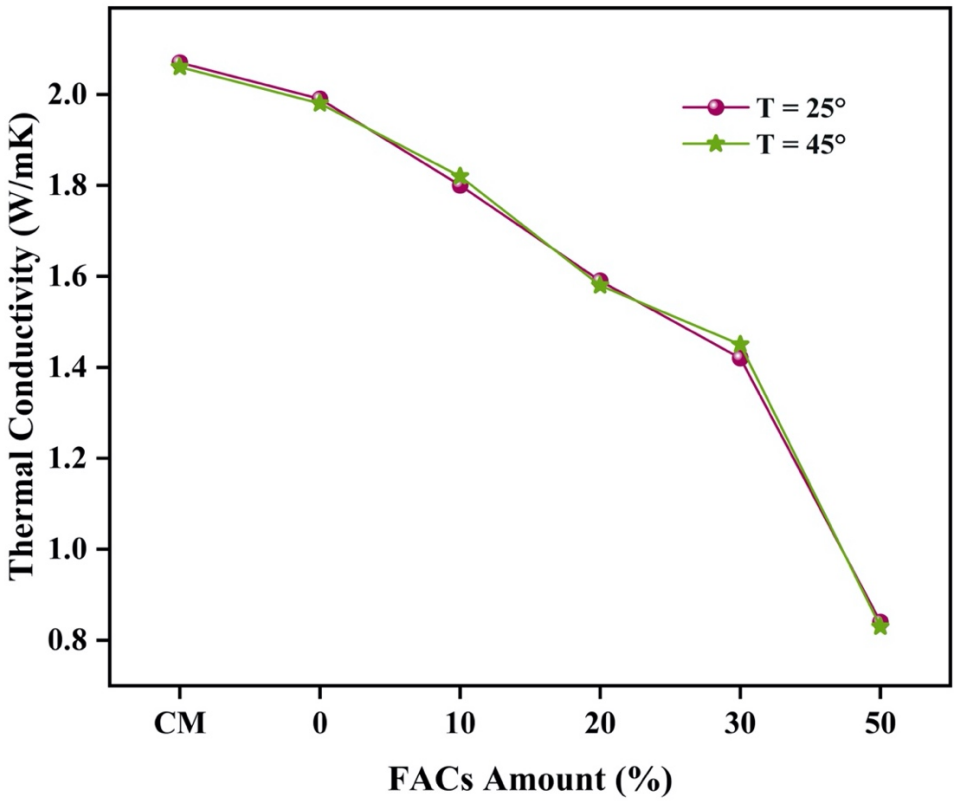

Figure 15 Effect of FACs content on the thermal conductivity of the mortar mixtures at 1.5 wt. % RMA

2.4.6. Printing Simulation

The intended goal was to have an extrudable cement-based material that can withstand the loading of the consecutive layers without consolidating or failing, in both the fresh and hardened states. To meet these criteria, we put the RMA to the test, we used the FAC-20 mortar mixture that exhibited desirable behavior in 3D-printing in terms of extrusion and buildability. This mixture had a negligible slump, had a shear-thinning behavior, displayed an acceptable specific strength and high thermal insulation. A 60 mL sterilized syringe was used to imitate the extrusion conditions, and the results were successful. As can be seen in Figure 16, the layers were homogeneous, crack-free, and did not exhibit macroporosity. Upon stacking multiple layers on top of each other, there was no visible consolidation, neither immediately nor overtime.

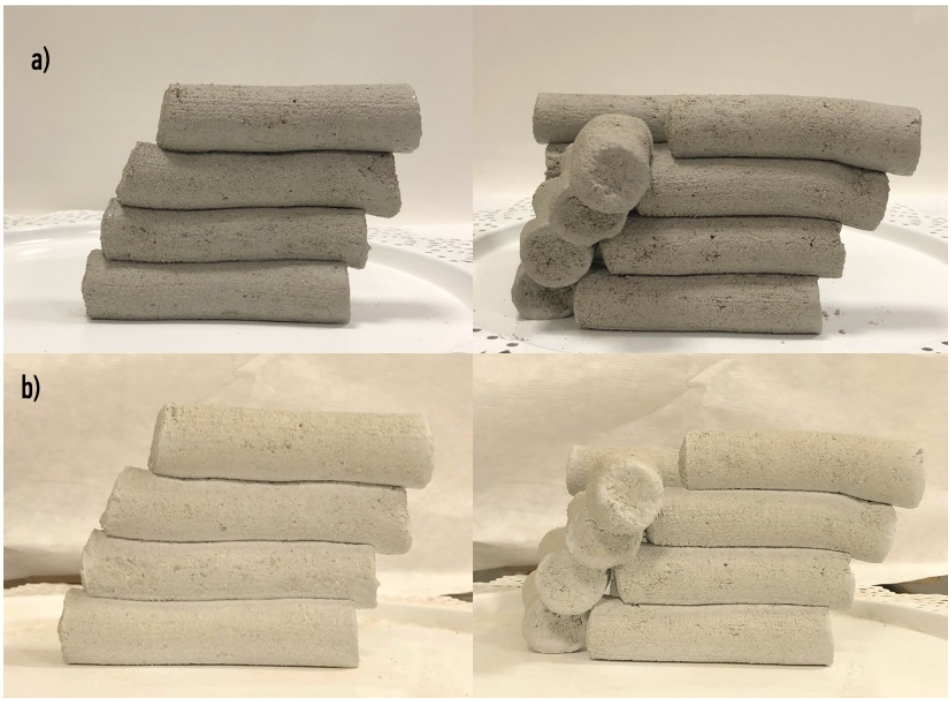

Figure 16 Extrusion of the FAC-20 mixture using a 60-ml medical syringe a) fresh and b) 365 days later

2.5. Conclusion & Future Work

The compatibility of the optimized rheology-modifying additive with the reactive particles facilitated the use of a higher amount of SCMs up to 38% while maintaining a homogeneous and crack-free mixture. Due to this modified rheology, the high content of SCMs met both lightweight (1900 kg/m^3) and high strength (80 MPa) criteria, as well as the possibility for extrusion through a nozzle of suitable sizes (≥ 2 cm).

Future studies shall include testing of this formulation with a large-scale printer to confirm its usability, lack of consolidation under self-weight, stability, and adequate printable strength, both the green and hardened strengths. Additionally, the use of reinforcing fibers can be assessed to increase the tensile strength and allow the printability of large-scale structures.

2.6. References

[1] M. Moini, J. Olek, J. P. Youngblood, B. Magee, and P. D. Zavattieri, "Additive Manufacturing and Performance of Architectured Cement-Based Materials," *Adv. Mater.*, vol. 30, no. 43, p. 1802123, 2018.

[2] C. Gosselin, R. Duballet, P. Roux, N. Gaudillière, J. Dirrenberger, and P. Morel, "Large-scale 3D printing of ultra-high performance concrete - a new processing route for architects and builders," *Mater. Des.*, vol. 100, pp. 102–109, 2016.

[3] D. Lowke, E. Dini, A. Perrot, D. Weger, C. Gehlen, and B. Dillenburger, "Particle-bed 3D printing in concrete construction – Possibilities and challenges," *Cem. Concr. Res.*, 2018.

[4] R. A. Buswell, W. R. Leal de Silva, S. Z. Jones, and J. Dirrenberger, "3D printing using concrete extrusion: A roadmap for research," *Cem. Concr. Res.*, vol. 112, pp. 37–49, 2018.

[5] F. Bos, R. Wolfs, Z. Ahmed, and T. Salet, "Additive manufacturing of concrete in construction: potentials and challenges of 3D concrete printing," *Virtual Phys. Prototyp.*, vol. 11, no. 3, pp. 209–225, 2016.

[6] Y. W. D. Tay, B. Panda, S. C. Paul, N. A. Noor Mohamed, M. J. Tan, and K. F. Leong, "3D printing trends in building and construction industry: a review," *Virtual and Physical Prototyping*. 2017.

[7] D. Marchon, S. Kawashima, H. Bessaies-Bey, S. Mantellato, and S. Ng, "Hydration and rheology control of concrete for digital fabrication: Potential admixtures and cement chemistry," *Cem. Concr. Res.*, vol. 112, pp. 96–110,

2018.

[8] S. Lim *et al.*, “Development of a viable concrete printing process,” in *Proceedings of the 28th International Symposium on Automation and Robotics in Construction, ISARC 2011*, 2011.

[9] T. Wangler *et al.*, “Digital Concrete: Opportunities and Challenges,” *RILEM Tech. Lett.*, vol. 1, p. 67, 2016.

[10] P. Foteinopoulos, V. Esnault, G. Komineas, A. Papacharalampopoulos, and P. Stavropoulos, “Cement-based additive manufacturing: experimental investigation of process quality,” *Int. J. Adv. Manuf. Technol.*, vol. 106, no. 11–12, pp. 4815–4826, 2020.

[11] G. Cesaretti, E. Dini, X. De Kestelier, V. Colla, and L. Pambaguian, “Building components for an outpost on the Lunar soil by means of a novel 3D printing technology,” *Acta Astronaut.*, 2014.

[12] S. C. Paul, G. P. A. G. van Zijl, and I. Gibson, “A review of 3D concrete printing systems and materials properties: current status and future research prospects,” *Rapid Prototyp. J.*, vol. 24, no. 4, pp. 784–798, 2018.

[13] I. F. Ituarte, E. Coatanea, M. Salmi, J. Tuomi, and J. Partanen, “Additive Manufacturing in Production: A Study Case Applying Technical Requirements,” in *Physics Procedia*, 2015.

[14] S. Cho, J. Kruger, S. Zeranka, and G. Van Zijl, “3D Printable Concrete Technology and Mechanics,” vol. 158, no. September, pp. 11–18, 2019.

[15] B. Lu *et al.*, “A systematical review of 3D printable cementitious materials,” *Construction and Building Materials*. 2019.

[16] L. Cassar, C. Pepe, G. Tognon, G. L. Guerrini, and R. Amadelli, “White Cement for Architectural Concrete , Possessing Photocatalytic Properties,” *11th Int. Congr. Chem. Cem.*, 2003.

[17] K. Moresová and F. Škvára, “White cement - Properties, manufacture, prospects,” *Ceram. - Silikaty*, vol. 45, no. 4, pp. 158–163, 2001.

[18] J. Bolden, T. Abu-Lebdeh, and E. Fini, “Utilization of recycled and waste materials in various construction applications,” *Am. J. Environ. Sci.*, 2013.

[19] T. T. Le, S. A. Austin, S. Lim, R. A. Buswell, A. G. F. Gibb, and T. Thorpe, “Mix design and fresh properties for high-performance printing concrete,” *Mater. Struct. Constr.*, 2012.

[20] C. Bedard and N. P. Mailvaganam, “The Use of Chemical Admixtures in Concrete. Part II: Admixture-Admixture Compatibility and Practical Problems,” *J. Perform. Constr. Facil.*, 2006.

[21] E. Ghafari, S. Ghahari, D. Feys, K. Khayat, A. Baig, and R. Ferron, “Admixture compatibility with natural supplementary cementitious materials,” *Cem. Concr. Compos.*, 2020.

[22] O. Akhlaghi *et al.*, “Modified poly(carboxylate ether)-based superplasticizer for enhanced flowability of calcined clay-limestone-gypsum blended Portland cement,” *Cem. Concr. Res.*, vol. 101, no. September, pp. 114–122, 2017.

[23] British Standards Institution BSI, “BS EN 197-1: Cement, Part 1: Composition, Specifications and Conformity Criteria for Common Cements,” *Br. Stand.*, 2011.

[24] J. Plank and O. T. Salami, “Synthesis, Effectiveness, and Working Mechanism of Humic Acid-{sodium 2-acrylamido-2-methylpropane sulfonate-co-N,N-dimethyl acrylamide-co-acrylic acid} Graft Copolymer as High-Temperature Fluid Loss Additive in Oil Well Cementing,” *J. Appl. Polym. Sci.*, vol. 126, no. 4, pp. 1449–1460, 2011.

[25] O. Akhlaghi, O. Akbulut, and Y. Z. Menceloglu, “Extensional rheology and stability behavior of alumina suspensions in the presence of AMPS-modified polycarboxylate ether-based copolymers,” *Colloid Polym. Sci.*, no. 293, pp. 2867–2876, 2015.

[26] S. H. Lu, G. Liu, Y. F. Ma, and F. Li, “Synthesis and application of a new vinyl copolymer superplasticizer,” *J. Appl. Polym. Sci.*, vol. 117, no. 1, pp. 273–280, 2010.

[27] B. Mather and W. Hime, “AMOUNT OF WATER REQUIRED FOR COMPLETE HYDRATION OF PORTLAND CEMENT,” *Concr. Int.*, 2002.

[28] ASTM, “C 305 – 06 ‘Standard Practice forMechanical Mixing of Hydraulic Cement Pastes and Mortars of Plastic Consistency,’” *ASTM Stand. B.*, 2015.

[29] B. Standards, “BS EN 196-1: Methods of testing cement — determination of strength,” 2005.

[30] A. Hot Disk, “Hot Disk Thermal Constants Analyser Instruction Manual.” pp. 1–138, 2016.

[31] A. Zingg, F. Winnefeld, L. Holzer, J. Pakusch, S. Becker, and L. Gauckler, “Adsorption of polyelectrolytes and its influence on the rheology, zeta potential, and microstructure of various cement and hydrate phases,” *J. Colloid Interface Sci.*, vol. 323, no. 2, pp. 301–312, 2008.

[32] J. D. Clogston and A. K. Patri, “Zeta potential measurement.,” in *Methods in molecular biology (Clifton, N.J.)*, Springer Science+Business Media, 2011, pp. 63–70.

[33] K. H. Khayat and A. Yahia, “Simple Field Tests to Characterize Fluidity and Washout Resistance of Structural Cement Grout,” *Cem. Concr. Aggregates*, vol. 20, no. 1, pp. 145–156, 1998.

[34] British standard, “Methods of test for mortar for masonry —Part 3: Determination of consistence of fresh mortar (by flow table),” *Bs En 1015-31999*, 2006.

[35] BSI Standards Publication, “BS EN 1015-10:1999 - Methods of Test for Mortar for Masonry - Part 10: Determination of dry bulk density of hardened mortar,” vol. 3, no. 1, 2006.

[36] E. Standard, “BS EN 12664:2001 Thermal performance of building materials and products — Determination of thermal resistance by means of guarded hot plate and heat flow meter methods — Dry and moist products of medium and low thermal resistance,” vol. 3, no. 1, pp. 1–55, 2001.

[37] S. E. Pagola, M.A., Jensen, R..L., Madsen, S., Poulsen, “measurement of thermal properties of soil and concrete samples.,” 2017.

[38] T. Tadros, “Electrostatic and Steric Stabilization of Colloidal Dispersions,” in *Electrical Phenomena at Interfaces and Biointerfaces: Fundamentals and Applications in Nano-, Bio-, and Environmental Sciences*, 1st ed., H. Ohshima, Ed. John Wiely & Sons Inc., 2012, pp. 1–20.

[39] K. Yoshioka, E. Sakai, M. Daimon, and A. Kitahara, “Role of steric hindrance in the performance of superplasticizers for concrete,” *J. Am. Ceram. Soc.*, vol. 80, no. 10, pp. 2667–71, 1997.

[40] Y. Li, H. He, Y. Ma, Y. Geng, and J. Tan, “Rheological and mechanical properties of ultrahigh molecular weight polyethylene/high density polyethylene/polyethylene glycol blends,” *Adv. Ind. Eng. Polym. Res.*, vol. 2, no. 1, pp. 51–60, 2019.

[41] B. Lu *et al.*, “Designing spray-based 3D printable cementitious materials with fly ash cenosphere and air entraining agent,” *Constr. Build. Mater.*, vol. 210, pp. 1073–1084, 2019.

[42] I. M. Krieger and T. J. Dougherty, “A Mechanism for Non-Newtonian Flow in Suspensions of Rigid Spheres,” *Trans. Soc. Rheol.*, vol. 173, no. 3, pp. 137–152, 1959.

[43] S. Guriyanova, V. G. Mairanovsky, and E. Bonaccurso, “Superviscosity and electroviscous effects at an electrode/aqueous electrolyte interface: An atomic force microscope study,” *J. Colloid Interface Sci.*, vol. 360, no. 2, pp. 800–4, 2011.

[44] K. Ishikiriyama, M. Todoki, and K. Motomura, “Pore size distribution (PSD) measurements of silica gels by means of differential scanning calorimetry. i. optimization for determination of psd,” *J. Colloid Interface Sci.*, vol. 171, no. 1, pp. 92–102, 1995.

[45] C. Li and M. Akinc, “Role of bound water on the viscosity of nanometric alumina suspensions,” *J. Am. Ceram. Soc.*, vol. 88, no. 6, pp. 1448–54, 2005.

[46] Z. Wu, C. Shi, and K. H. Khayat, “Influence of silica fume content on microstructure development and bond to steel fiber in ultra-high strength cement-based materials (UHSC),” *Cem. Concr. Compos.*, vol. 71, pp. 97–109, 2016.

[47] J. K. Weng, B. W. Langen, and M. A. Ward, “Pozzolanic reaction in Portland cement, silica fume, and fly ash mixtures,” *Can. J. Civ. Eng.*, vol. 24, no. 5, pp. 754–760, 1997.

[48] F. Liu, J. Wang, X. Qian, and J. Hollingsworth, “Internal curing of high performance concrete using cenospheres,” *Cem. Concr. Res.*, vol. 95, pp. 39–46, 2017.

[49] K. Senthamarai Kannan, L. Andal, and M. Shanmugasundaram, “An investigation on strength development of cement with cenosphere and silica fume as pozzolanic replacement,” *Adv. Mater. Sci. Eng.*, 2016.

[50] H. G. Russell, “ACI Defines High-Performance Concrete,” *Concr. Int.*, vol. 21, no. 2, pp. 56–57, 1991.

[51] American Concrete Institute, *Aci Concrete Terminology, ACI CT-13*. Farmington Hills, MI, 2013.

[52] T. T. Le *et al.*, “Hardened properties of high-performance printing concrete,” *Cem. Concr. Res.*, vol. 42, pp. 558–566, 2012.

[53] A. Hanif, Z. Lu, and Z. Li, “Utilization of fly ash cenosphere as lightweight filler in cement-based composites – A review,” *Constr. Build. Mater.*, vol. 144, pp. 373–384, 2017.

[54] C. C. Ban and M. Ramli, “Optimization of Mix Proportion of High Performance Mortar for Structural Applications Cheah Chee Ban and Mahyuddin Ramli Sustainable Housing Research Unit , School of Housing , Building and Planning ,” *Concrete*, vol. 3, no. 4, pp. 643–649, 2010.

[55] V. Rheinheimer *et al.*, “Multi-scale study of high-strength low-thermal-conductivity cement composites containing cenospheres,” *Cem. Concr. Compos.*, vol. 80, pp. 91–103, 2017.

[56] M. V. Deepthi, M. Sharma, R. R. N. Sailaja, P. Anantha, P. Sampathkumaran, and S. Seetharamu, “Mechanical and thermal characteristics of high density polyethylene-fly ash Cenospheres composites,” *Mater. Des.*, vol. 31, no. 4, pp. 2051–2060, 2010.

CHAPTER 3

A MODIFIED COPOLYMER COAGULANT FACILITATES GREEN BODY MACHINABILITY OF CERAMICS

3.1. Introduction

Yttria-stabilized zirconia (YSZ) is a high strength, high stiffness, high thermal conductivity, high hardness, and wear- and chemical-resistant material [1–3]. YSZ is frequently used in dental and biomedical applications among other more industrial uses such as solid oxide fuel cell electrolyte, high thermal applications, and thermocouple shielding [4–10]. Such applications of YSZ are restricted due to the difficulties in its precision machining in the sintered state [11]. The rather high hardness of YSZ results in faster machining tool wear and thus requires complex techniques such as ultrasonic drilling, high-speed milling process, and laser and thermally-assisted machining [12–16]. Green machining of YSZ has been explored to achieve i) lower energy consumption, ii) high material removal rate, iii) applicability of mold-free rapid tooling, iv) freedom of the type of operation like drilling and lathing, as opposed to only grinding in the sintered state, v) the near-net-shape forming —close to the size/shape of the final desired product, and vi) minimized tool wear especially for diamond-coated tools [17–21].

Recent advances in ceramic casting have made it possible to machine ceramics like alumina and zirconia in their green body state [21, 22]. The modified techniques involved direct ceramic machining of ceramics objects that were fired to the pre-sintered state (≈1000 ˚C) or machining of ceramics cast at much lower temperatures (40–80 ˚C) [23–26]. Colloidal forming of ceramics by consolidation made it possible to cast highly homogeneous and high solid-ratio ceramic green bodies at lower temperatures without the need for cold isostatic pressure [27, 28]. Easier molding and demolding processes

were additional advantages of colloidal forming. Direct consolidation of ceramics can be achieved by several different methods including but not limited to: gelcasting, freeze/dry casting, colloid-based processes such as direct coagulation casting (DCC), protein coagulation casting (PCC), thixotropic casting, and temperature-induced forming [29–33]. Different methods rely on different interactions of particles: to form a strong green body, gelcasting depends on the crosslinking of monomers/ polysaccharides/ starch/ cellulose derivatives [29, 34]. After they are added to the suspension, the crosslinking takes place with the help of a compatible initiator and heat. Other methods like DCC and PCC are based on the surface science and flocculation of the suspension. The coagulation is attained by destroying the electrical double layer of the particles by adjusting the pH to the isoelectric point by increasing the electrolyte concentration or inducing enzyme reactions [32, 34, 35]. Nevertheless, these techniques, along with injection molding and slip casting, still require heat, the use of molds for precise machining after casting, or high amounts of binders.

On the other hand, flocculation or agglomeration of particles that is achieved by the addition of polymers is employed in solid-liquid phase separation for applications pertinent to water treatment [36]. The ease of separation is governed by both the floc growth and the destabilization of the colloidal suspension [37]. This mechanism leads to the sedimentation/settlement or floating of the particles within the liquid phase. In this case, the flocculation of the particles is provided by polymer bridging or patching mechanisms onto the particles [37, 38].

However, if the added polymer covers the particle and maintains the stabilization and liquid retention while promoting polymer-polymer bridging, then the separation of the phases does not occur [40]. Instead, only the floc growth takes place without the destabilization of the suspension. Observably, the viscosity of the suspension increases, and its consistency becomes dough-like —pliable and malleable. We found this process to be based mainly on the compatibility of the designed polymer with the particles, the weight percentage of the added polymer as a coagulant as well as the liquid retention capabilities.

To our knowledge, this stable coagulation phenomenon has not been explored yet in the colloidal consolidation forming of ceramics. In this chapter, we report a novel DCC technique that employs the polymer-polymer bridging mechanism without inducing phase destabilization. To achieve that, we synthesized a set of linear copolymers consisting of, 2-Acrylamido 2-methylporpane sulfonic acid (AMPS) and Acrylic Acid

(AA) at different molar ratios. This technique facilitated precise green machining of 40 nm-sized 3 mol % YSZ in its dry state that was carried out entirely at room temperature, from casting to the finished machined unsintered product. The optimum linear copolymer was used in minimum amounts as a coagulant in an otherwise neat 65 wt. % YSZ suspension. It instantly coagulated the suspension and eliminated the need to use a binder, thus eliminating the binder burnout step during sintering. To study the stability of the suspensions, we performed electrokinetic characterization: direct light scattering (DLS) and zeta potential measurement. To observe the floc growth, we carried out rheological characterization and measured the increase in size by a particle size analyzer. To test the green machinability, we drilled different sized holes of 0.6–2 mm in samples dried at room temperature. This work underlines the enhanced fresh properties, malleability, and ease-of-production of the dense green and sintered bodies, which was made possible by employing a linear copolymer, at 1%. This additive enabled the instantaneous coagulation of 65 wt. %, 3 mol % YSZ suspensions by bridging the nanoparticles.

3.2. Materials & Methods

3.2.1. Materials

Spherical 40 nm-sized 3 mol yttria-stabilized zirconia, with a specific surface area of 10–25 m^2/g and density of 5.88–5.91 g/cm^3 was purchased from US Research Nanomaterials, Inc. The monomers AA (99%), AMPS (99%) and the chemicals NaOH (97%), HCl (37%), and KPS (≥ 99%) were used to synthesize the polymers, and their Mw's are given in Table 2.2.1 under section 2.2.1 in the second chapter. Additionally, Vinylphosphonic Acid (VPA, 97%) monomer with Mw of 108.03 g/mol was purchased from Acros Organics, Germany.

3.2.2. Design the Single Additive

3.2.2.1.Synthesis

To synthesize random blocks of linear copolymers of the monomers AA and AMPS, free-radical polymerization of the monomers was set up [41]. Firstly, the synthesis conditions were optimized to maximize the possibility of procuring polymers with Mws in the range of 10–50K g/mol. This was achieved by choosing the initiator

concentration to be 2 g /50 mL or 4 g/ 100 mL and the total water amount, in which the monomers are dissolved, to be 175–200 mL. Table 3.2.1 displays the molar feed ratios of AA/AMPS that are selected for this study. The monomers were dissolved in water first and their pH was adjusted to 8 using 12M, 2M, 1M, and 0.1 M NaOH and 0.1M HCl. Then, the solutions were poured into 500 mL 2-neck or 3-neck flasks and connected to reflex condensers. The temperature was increased to 50 ˚C and N_2 gas was purged to remove free oxygen from the system. Meanwhile, the initiator solution was prepared, and its pH was also adjusted to 8 to prevent a significant shift in the pH level of the main solution. The initiator was added at once at T = 50 ˚C and the temperature was then increased to T = 80 ˚C where the synthesis continued for 6 hours. Homopolymer AA and homopolymer AMPS were synthesized in the same manner. Nevertheless, AA/VPA and homopolymer VPA were synthesized as follows; the monomer(s) were first dissolved in 50 mL water and stirred for 3 hours, then the pH was adjusted to 8 with about 30 mL of NaOH. At T = 60 ˚C, 0.3 g/ 10 mL initiator was added, and the temperature was increased to 80 ˚C after which the synthesis was carried out for 4 days.

Table 3.2.1 Characteristic properties of the synthesized linear copolymers

Molar Concentration (AA/AMPS)	Molar feed ratio (AA/AMPS)	Polymer acronym	AA/AMPS[4]	Number Average Molecular Weight, M_n (g/mol)[5]	PDI (Mw/Mn)[5]
0.2;0	100	AA100	1	13032	1.54
0.1;0.1	50/50	AMPS50	1/1.28	27512	1.06
0;0.2	100	AMPS100	1	12480	1.59
0.1;0.1	50/50	AMPS50-2	1/1.1	11581	1.34
0.1;0.1	50/50	AMPS50-3	1/0.82	19941	1.23
0.1;0.1	50/50	AMPS50-4	1/0.7	42589	1.07
0;0.2	100	VPA100	1	2511	1.03
0.1;0.1	50/50	VPA50	1/1.3	87604	2.34

[4] Determined by NMR
[5] Determined by GPC

3.2.2.2.Titration

Titration of AA100, AMPS50, and AMPS100 that was carried out with a pH meter, Ohaus Starter300 is given in Figure 17. The concentration of all the solutions was 1mg/1mL where 0.1 M HCl was used to adjust the starting pH to 2, then, 0.1 M NaOH was added in micrometer increments, 10–200 μL, as the titrant.

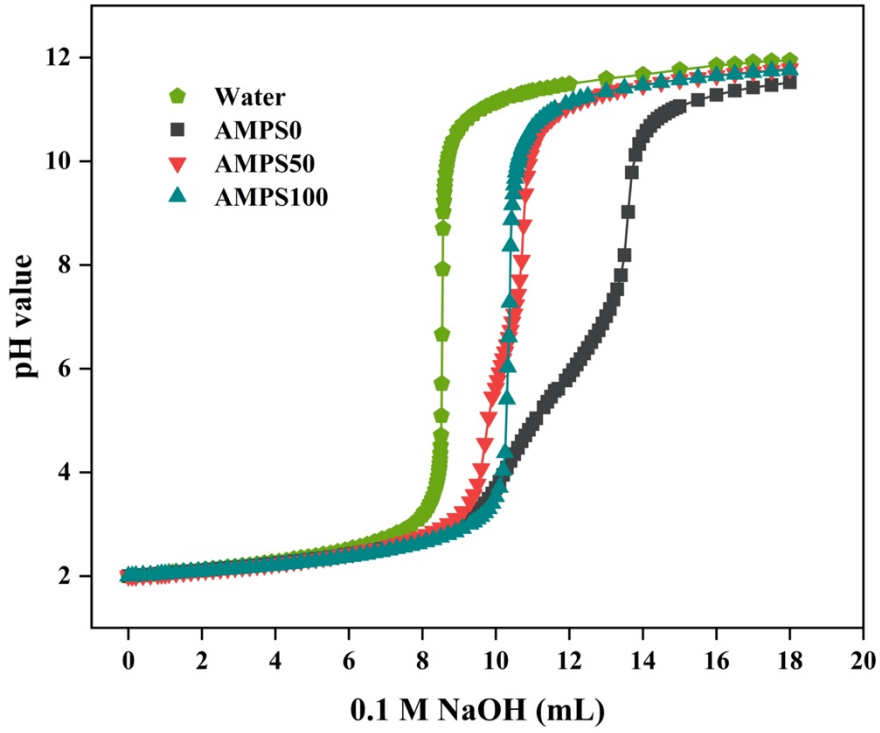

Figure 17 Sodium hydroxide titration of the copolymer solutions at 1 mg/ 1mL

3.2.2.3.Nuclear Magnetic Resonance (NMR)

All the linear copolymers were precipitated with acetone and dried overnight at 70 ˚C in a vacuum. 20 mg of each of the solid copolymers were dissolved in D_2O for the proton ^{1}H-NMR test using Varian Unity Inova 500 MHz spectrometer. The molar concentrations of each copolymer were then calculated based on the integral of the peaks and their shift

3.2.2.4.Gel Permeation Chromatography (GPC)

To measure the molecular weights Mn and Mw of the synthesized copolymers, solid copolymers were dissolved in aqueous solutions of 0.14M NaCl, 0.01 M, $NaNO_3$, and 0,.01M Na_2HPO_4. Agilent 1260 Infinity was employed with a flow rate of 0.7 mL/min.

3.2.3. Electrokinetic Characterization

To measure the zeta potential of the neat YSZ and study the effect of the copolymers on the surface charge of the particles, suspensions with a low concentration of 0.4 wt. % (4 mg powder in 100 mL DI water) were prepared. Sonication was carried out for 15 min under a controlled temperature range of 19–21 ˚C, after that the beakers were moved to the magnetic stirrers. 0.25 wt. % increments of 10 mg/100 mL copolymer solutions were added gradually into the YSZ suspensions. The cuvettes were then filled while making sure no bubbles were formed and immediately inserted into the device, Zetasizer Nanoseries, Malvern Instrument. All measurements were taken at 25 ˚C by applying Smoluchowski approximation. The final reported value is the average of 6 measurements with 12–100 runs each.

To characterize the size of the particles both before and after the addition of each of the copolymers, Direct Light Scattering (DLS) at a 173˚ backscatter measurement angle was operated using the same device. Ultra-low concentrations of 0.0025 wt. % (1 mg powder/ 400 mL DI water) were prepared. These samples were sonicated for 2 hours, again with a controlled temperature range of 19 ˚C to 24 ˚C maximum. After sonication, the samples were magnetically stirred while the disposable cuvettes were filled, the measurements were immediately taken after that. The final reported value of six measurements of the hydrodynamic diameter (Z-average) were obtained at 0, 0.2, 0.5, 1, 1.25, 1.5, 2, 2.5 & 3% of the added copolymer.

3.2.4. Size Characterization by Particle Size Analyzer

In addition to DLS, the variation in the particle/flocs size of suspensions at a more concentrated loading was tested via a particle size analyzer (PSA), Mastersizer 3000, Malvern Instruments. Neat suspensions of 1 wt. % and 30 wt. % were tested to obtain the floc sizes and were superimposed to report any differences. 1 wt. % of AMPS50 was selected to show its effect in growing the size of YSZ particle colonies with different suspension loading. All colloids were sonicated for 1 hour with a controlled temperature range of 19–24 ˚C. After sonication, the samples were magnetically stirred until the measurements were taken. Micro drops from the samples were put into the active stirrer of the device, Hydro SM, to get an obscuration of a maximum of 20%. Six measurements that ran for 30 seconds each were recorded and their average was reported in the final results.

3.2.5. Rheological Characterization

The samples for this test were prepared at 45 wt. % solid particles loading because it was the closest concentration to the highest loading, which also maintained liquid/fluid consistency for the entire set of copolymers. To measure the change in viscosities of the suspensions with different shear rates, the test was carried out using Anton Paar MCR302 rheometer. With a cone and plate geometry, the gap size was fixed at 0.15 mm and the temperature was fixed at 25 ˚C during all the measurements. The viscosity was first measured at a constant shear rate of 100 s^{-1} for 20 seconds. Then, it was measured with decreasing shear rate from 100 s^{-1} to 1 s^{-1} for 23 seconds and increasing shear from 1 s^{-1} to 100 s^{-1} for another 23 seconds.

3.2.6. Cracking and Malleability in Wet State

The malleability, the drying, and the cracking of the YSZ dough samples were quantified at 1 wt. % addition of AA100, AMPS100, and AMPS50 by measuring the variation in the solid content with time. 65 wt. % YSZ suspensions were first prepared, and the copolymer was added next to coagulate the particles. After that, small amounts were taken and shaped into balls by hand and then pushed into a mold to take the shape of a disk of 5 mm height and 10 mm diameter. Immediately after that, the samples were pushed out of the mold onto a plexiglass piece. During the preparation of each specimen, the suspension was covered with parafilm to prevent undesired evaporation of water. The time was recorded after each specimen was shaped and let dry at room temperature up to the measurement time. After that, the solid content measurements were taken in intervals of 0–360 minutes based on this recorded initial time. Solid content device was used to obtain the results in wt. %, it heated up to 150 ˚C, and the final reported value was the moisture content, which was calculated as 100 – solid content. Additionally, pictures of the wet samples were taken to demonstrate the effect of each copolymer on the malleability.

3.2.7. Green Body Machinability

The samples were first coagulated by adding 1 wt. % of each of AMPS50, AA100, AMPS100. The consistency of these samples was dough-like, which made it possible for it to be easily shaped or pressed into a mold by hand. A set of specimens were handled in their wet state by penetration with a 6 inches long stainless steel 316 syringe needle (Sigma Aldrich), as illustrated in Figure A1, a. Another set was formed with molds, or by hand, and left to dry at room temperature overnight. The dry green bodies were then drilled with Proxxon Bench Drill TBM 22O at 3500 rpm with different pin sizes of 0.6–5 mm. A dry rod of 10 cm length and 1 cm diameter was drilled with a TH2866 Legged Universal Lathe Machine at 480 rpm. Various mold sizes/shapes were designed on RDworks software and made by peck drilling of acrylic sheets.

3.2.8. Sintering

For sintering of all the samples, Protherm furnace (1600 ˚C capacity) was operated and programmed with the sintering profile that is demonstrated in Figure 18 below [42].

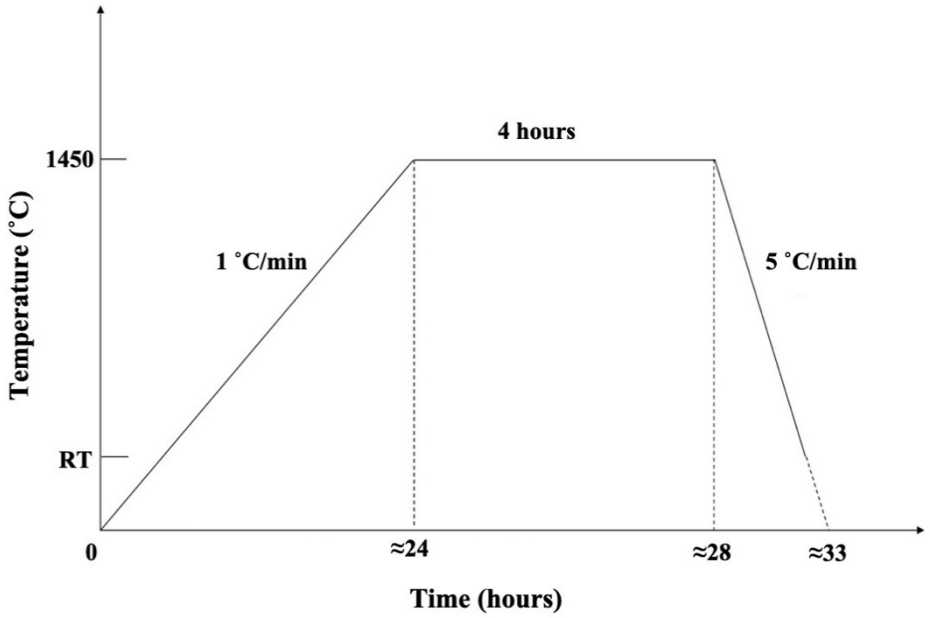

Figure 18 Sintering profile of the samples from RT to 1450 ˚C with one dwelling time interval of 4 hours

3.2.9. Linear Shrinkage

The samples were measured with an electric ruler after drying overnight and before sintering. Then, they were measured again, in the same direction, after sintering. For all directions, the shrinkage was calculated by:

$$\%S = \frac{L_{GB} - L_{SIN}}{L_{GB}} \times 100$$

Where %S is the dimensional shrinkage, L_{GB} is the length of the green body and L_{SIN} is the length of the sintered body [43].

3.2.10. Density

The density of the sintered samples was assessed by the Archimedes method. The sample was measured at 22 ˚C in air and while submerged underwater [44]. Then the density was calculated as follows:

$$\rho_{Sample} = \rho_{water}\left(\frac{M_{air}}{M_{air} - M_{wet}}\right)$$

Where ρ_{water}= 0.99777 g/cm^3 at 22 ˚C

3.2.11. SEM

The sintered samples were polished before taking SEM images. The polishing was done in stages starting with sandpapers of sizes 600, 1000, 1200, 2500, and 4000, and later with diamond suspensions of 6 µm, 1 µm, and 0.25 µm. Metkon Gripo V1 Grinder-Polisher was used with running water for polishing with sandpapers. Gold/platinum, 70/30 wt/wt, the coating was applied on the sample as a thin 10 nm layer for 40 sec, to prevent charging of the sample inside the SEM chamber. The surface morphology of one sintered sample was studied by taking an image at a magnification of 50K X, EHT of 1 kV, and a working distance of 4 mm.

3.2.12. Mechanical Strength

To prepare rectangular sintered samples of length, width, and height of 25×2×3 mm^3, sizes were according to the ASTM standards [45]. The same novel shaping technique was applied. Firstly, the obtained dough was formed by hand and then pushed into rectangular molds to take the shape of the mold. The molds were initially lubricated with olive oil; after the material placement, they were left open on both sides to allow for isotropic shrinkage and prevent buckling of the rod. Zwick/Roell Z100 Universal Testing Machine was employed for the 3-point bending test to procure the flexural strength of the sintered samples. The crosshead speed was set to 0.2 mm/min and the test was repeated 3 times and then the average of 3 specimens was taken as the final reported result.

3.3. Results & Discussion

3.3.1. Electrokinetic Characterization and Coagulation Mechanism

To evaluate the mechanisms that the linear copolymers induce when added to the YSZ system and to select an optimized copolymer, electrokinetic characterization was studied. Results were obtained and explained by the change in zeta potential and size of the YSZ flocs in the system, which demonstrated the relationship between the design of the copolymer, its added weight percentage, and its effect on the nanoparticles. Coagulation in the sense of increasing the size of particle colonies, while maintaining suspension stability and water retention, can be attributed to three main mechanisms, as depicted in Figure 19: i) Polymer dispersion at low percentages, ii) Copolymer-copolymer interaction at and around the optimum percentage, iii) Unadsorbed free copolymer-adsorbed copolymer interaction at higher percentages.

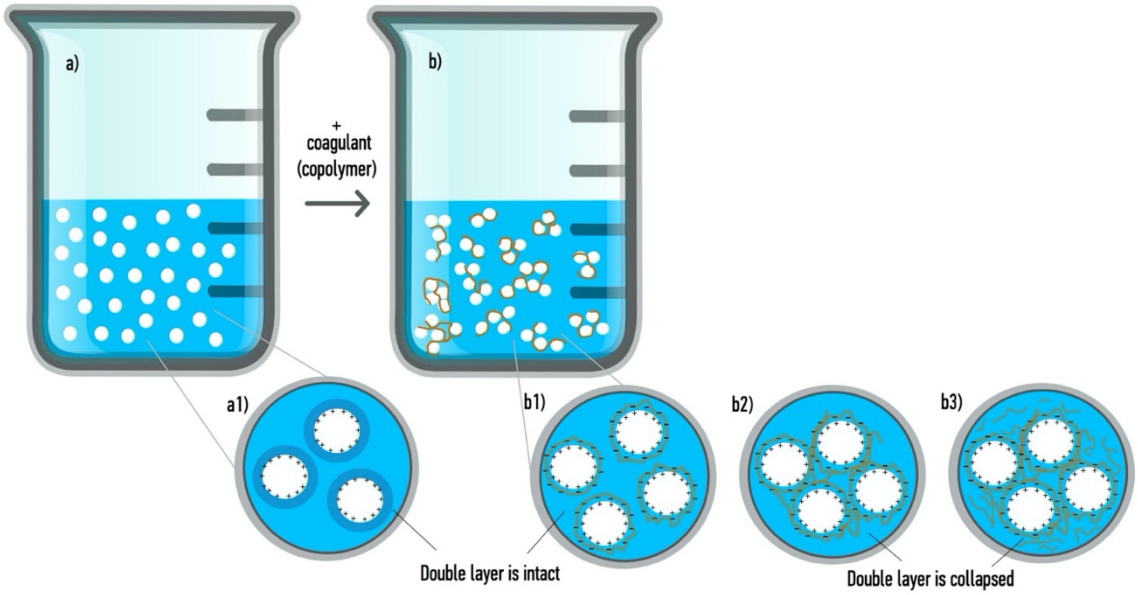

Figure 19 Coagulation mechanism of YSZ nanoparticles upon the addition of a linear copolymer: a1) stability of the colloidal particles in an aqueous solution before the addition of the coagulant, b1) Stability after adding the coagulant up to the optimum amount b2) At and beyond the optimum amount b3) At higher percentages

Starting with a neat YSZ suspension, Figure 19 a1, the suspension is stable, which is also confirmed by the high zeta potential value of +33 mV as per Figure 20. Since the surface charge of the YSZ particles in an aqueous solution is highly positive, electric repulsion is predominant via the electric double layer of the particles [46]. The principal

size of the particles is 40 nm, however, the reported value by DLS in Figure 21 was about 363 nm. This increase can be ascribed to the high activity of nanoparticles and their tendency to naturally agglomerate. For a maximum loaded suspension, at this level, the consistency of the material is thick but still liquid-like, thus there is no coagulation. Upon the addition of 0.2–0.5 wt. % of AMPS50, 0.75–1 wt. % of AMPS100, 1–1.25 wt. % of AA100, and 1.5–1.75 wt. % of VPA50, the negatively-charged copolymer chains adsorb onto the positively charged YSZ particles and fully cover their surface. This was understood from the shift of the zeta potential values from + 33 mV to –20 mV with AMPS50, –10 mV with AMPS100, and ≈ 0 mV with AA100 and VPA50 shown in Figure 20. This polymer-particle interaction is depicted in Figure 19 b1, at which, the electric double layer is still intact. Still, at this level the desired coagulation of the particles is incomplete, so we observed the behavior at higher percentages. For VPA50 and AA100 when the zeta is about 0 mV, the flocculation of the particles is governed by polymer-particle bridging, but the destabilization of the system causes poor shaping and water retention. At 1.25 wt. % addition of any of the copolymers, the coagulation occurs in maximum-loaded suspensions, Figure 19 b2 illustrates the copolymer-copolymer bridging at this value. Here, the zeta potential reached the last plateau region for AMPS50, AMPS100, and AA100, and reached the highest value at –30 mV with AMPS50. It is worth noting that AA100 and VPA50 both display the effect of the bilayer adsorption at low weight percentages, which is why a plateau, a jump, and another plateau are seen on the graph. Furthermore, the DLS results exhibit the change in the hydrodynamic diameter of the particles with increased copolymer content. The curves in Figure 21 display a decrease in size until an optimum value is achieved, where the copolymer-copolymer bridging occurs, and a rise beyond that point. Figure 19 b3 depicts this rise, which is due to the free copolymer that does not get adsorbed onto the fully covered particles after the optimum value. Compared to the homopolymers and VPA50, AMPS50 exhibited a higher absolute value of zeta potential and the lowest floc size of about 200 nm — a 40% drop in size from the neat colonies at 1.25 wt. %. The following sections on the rheology and malleability affirm the superior behavior of AMPS50 as the optimum copolymer in terms of achieving a stable coagulated suspension.

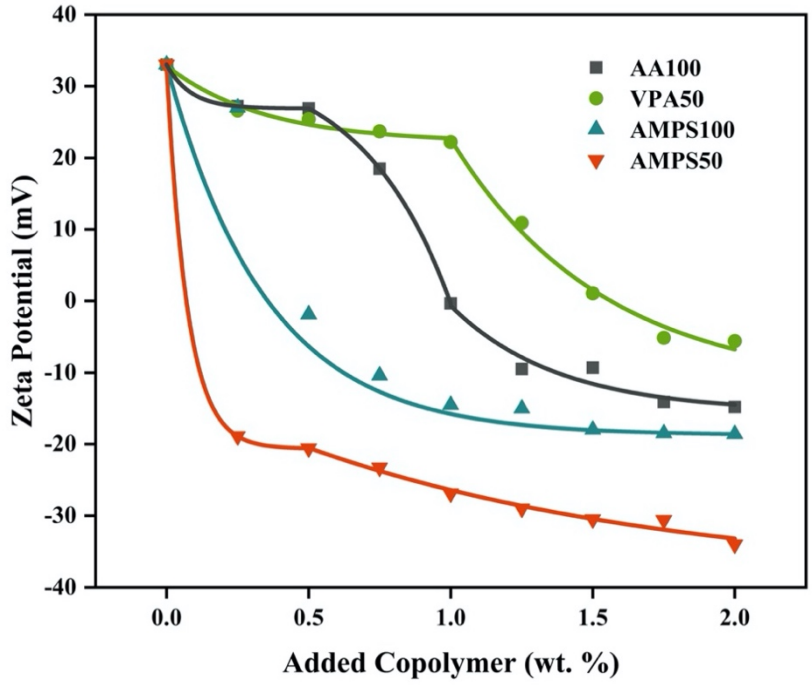

Figure 20 Zeta Potential of YSZ nanoparticles in the presence of different weight percentages of the linear copolymer at native pH

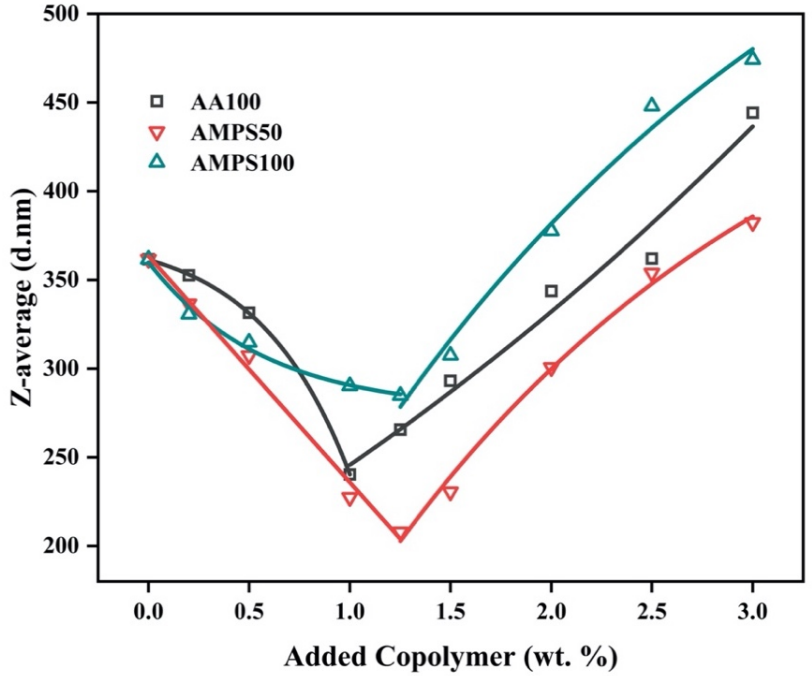

Figure 21 Size of the YSZ colonies measured by DLS in the presence of different copolymers at different weight percentages

3.3.2. Characterization of Size via Particle Size Analyzer

To investigate the size of the particles at higher loadings compared to the loading of 0.0025 wt. % at which the DLS measurements were taken, we tracked the sizes of 1 wt. % and 30 wt. % loaded suspensions via PSA. It can be observed from Figure 22 where both of the weight percentages are superimposed that they overlap over many of the points on the spectrum, where ≤ 50% of the particles were of sizes ≤ 1.5 μm and 1.63 μm for 1 wt. % and 30 wt. %, respectively. This behavior confirmed the reproducibility of the results at higher particle concentrations.

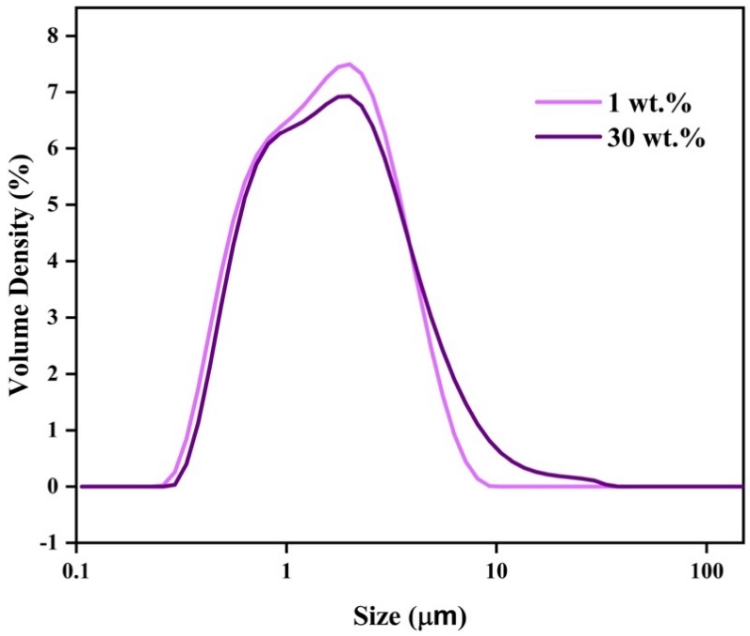

Figure 22 Size of the neat YSZ colonies measured by PSA at native pH

Moreover, Figure 23 displays the range of the spectra at different loadings, including DLS, in the presence of 1 wt. % of AMPS50; we selected this value as it is the closest to the optimum value of 1.25 wt. % at which the particle-particle interaction is avoided. The sharpness of the 0.0025 wt. % and 1 wt. % peaks represent the dispersing and stabilizing effect of the added copolymer. This sharpness, or volume intensity percent, softens with the 30 wt. % suspension as not only the size of the colonies increases but also their number. However, the size of the flocs did not shift between the two loadings. The small peak at about 9 µm on the DLS spectrum reveals the flocculation tendency caused by the addition of AMPS50.

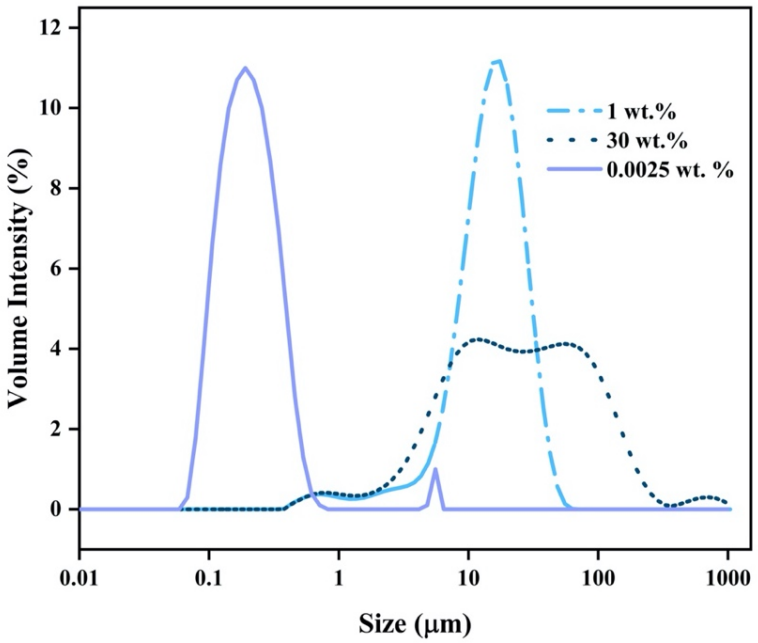

Figure 23 A comparison of the sizes of the YSZ colonies in the presence of 1 wt. % of AMPS50 at different loadings measured by DLS and PSA

3.3.3. Rheological Characterization

To satisfy the coagulation requirement of high viscosity without inducing destabilization of the particles in the suspension, we studied the rheological response of 45 wt. % YSZ with a set of copolymers at different percentages. In the absence of any copolymers, the neat suspension has a rather low viscosity of 0.1 Pa.s and is stable as proven by the neat zeta potential of +33 mV (Figure 20) as well. To synchronize the optimum values obtained by the electrokinetic characterization and to avoid excessive or insufficient copolymer addition, first, we tracked the viscosity as a function of shear rate of 0.5–5 wt. % of AMPS50. As can be seen in Figure 24, the minimum addition of 0.5 wt. % caused the viscosity to increase by approximately one order of magnitude. Beyond this point, there was another jump in the order of magnitude of viscosity in which the rest of the polymers flowed similarly up to 3 wt. %.

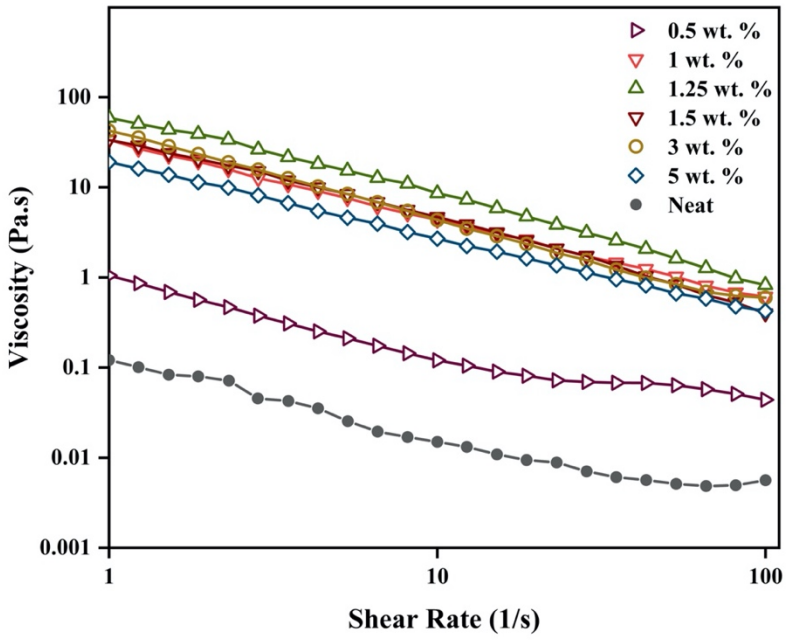

Figure 24 The effect of different AMPS50 percentages on 45 wt. % YSZ suspensions

The addition of 5 wt. % of AMPS50 slightly decreased the viscosity again, which can be attributed to the extra uncorrected water coming from the copolymer solution. All the curves had a decreasing slope with shear rate indicating shear thinning behavior. As there was not a significant difference in the viscosity, the value of 1 wt. % was satisfactory in attaining higher viscosity at the lowest amount of the additive. At this dosage in the presence of various polymers, we tracked the viscosity with a varying shear rate, as presented in Figure 25. AMPS50 had an intermediate viscosity between AMPS100 and AA100, which is anticipated as this copolymer will show the combined effect of the other two. AA100 displayed a much higher viscosity of several orders of magnitude, however, the reason the viscosity is so high at this dosage is that the zeta potential was around 0 mV (Figure 20). This meant that this weight percentage causes "pseudo" coagulation —undesirable flocculation of particles that is due to the destabilization of the suspension [47].

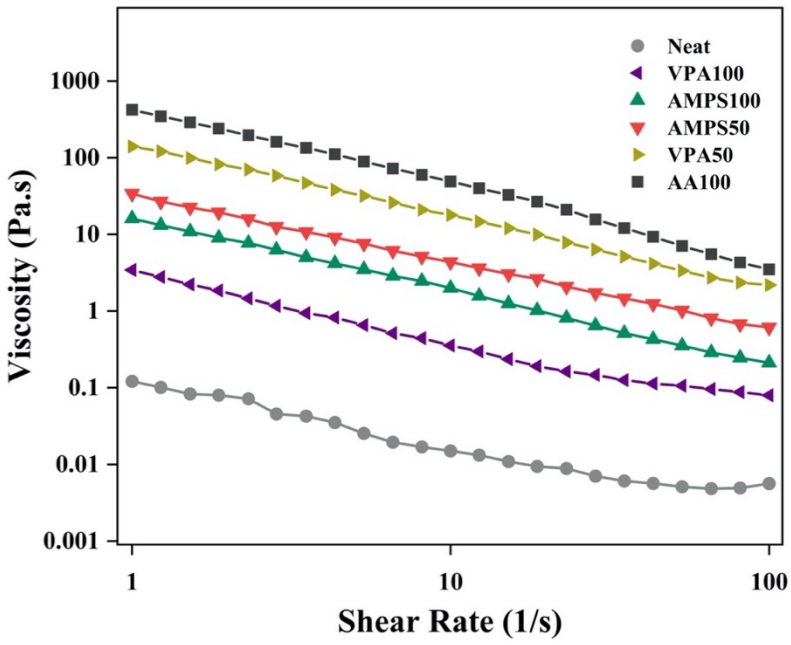

Figure 25 The effect of different linear copolymers on 45 wt. % YSZ suspensions at 1 wt. % addition

This is also evident by the shift in the order of magnitude at a dosage of 1.5 wt. % (Figure 26), in which the zeta potential was -10 mV. The homopolymer VPA100 did not have a considerable effect on the viscosity, at neither 1 wt. % nor 1.5 wt. %, this is because of its low Mw, which is due to the difficulty in polymerization. The increase of the viscosity by the addition of 1 wt. % of VPA50 can be partially due to the zeta potential drop by 33%, while at 1.5 wt. % the sudden increase was due to the pseudo coagulation effect. The difference in the rate of change between the AA100 and AMPS50 curves in Figure 26 elucidates a higher plastic viscosity provided by AMPS50 with a smaller slope.

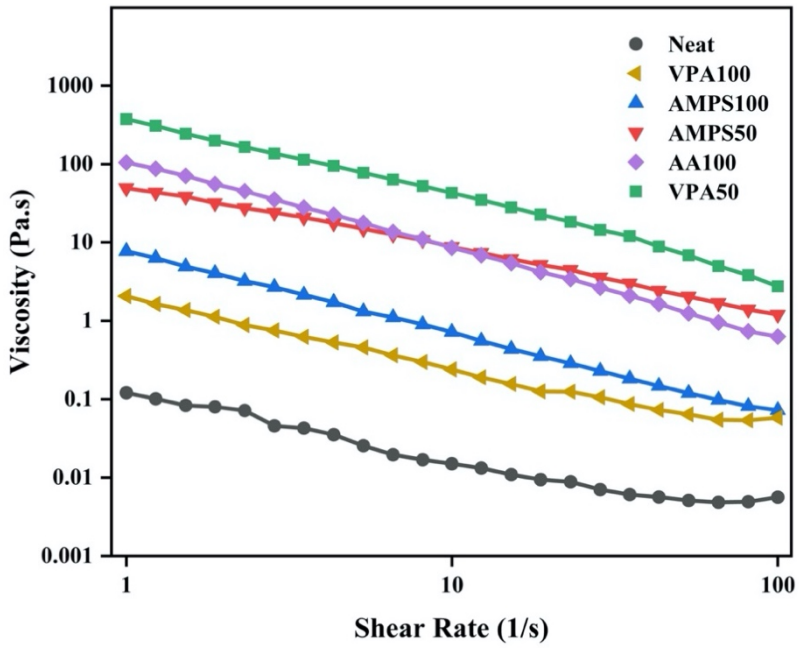

Figure 26 The effect of different linear copolymers on 45 wt. % YSZ suspensions at 1.5 wt. % addition

The previously discussed copolymer throughout the text had an Mw of 27.5 K g/mol, which was slightly higher than the homopolymers. Therefore, to assess the Mw effect on the viscosity of the suspensions and to eliminate the uncertainty that a higher Mw had a significant impact on the performance of the copolymer, we conducted the test on AMPS50 copolymers with a range of different molecular weights. Figure 27 distinctly demonstrates the inapplicability of Mw in terms of modifying the rheological response at this range of 11.5–42.5 K g/mol.

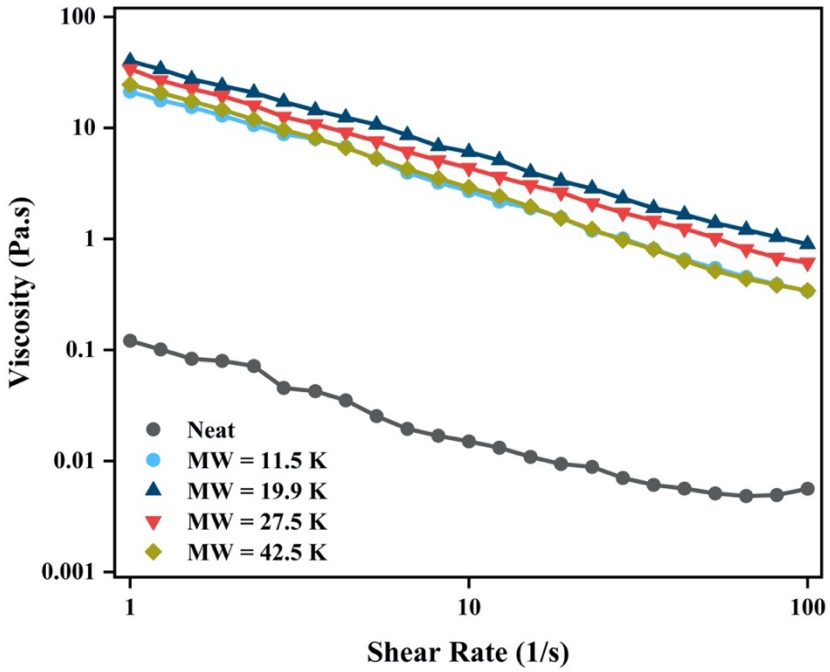

Figure 27 The effect of different Mws of AMPS50 on the rheology of 45 wt. % YSZ suspensions

3.3.4. Malleability and Cracking Behavior

To assess the malleability of the samples with a set of linear copolymers, AA100, AMPS100, AMPS50, and VPA50, we traced the cracking formation on wet samples during shaping and handling. The behavior can be characterized by the homogeneity, ease of shaping, cutting through, smoothening the surface, propagation of the crack, and the moisture content of the specimen. On the illustration given in

Figure 28, it can be clearly seen that all the samples had a homogeneous consistency, in that there was no liquid-solid phase separation after the coagulation.

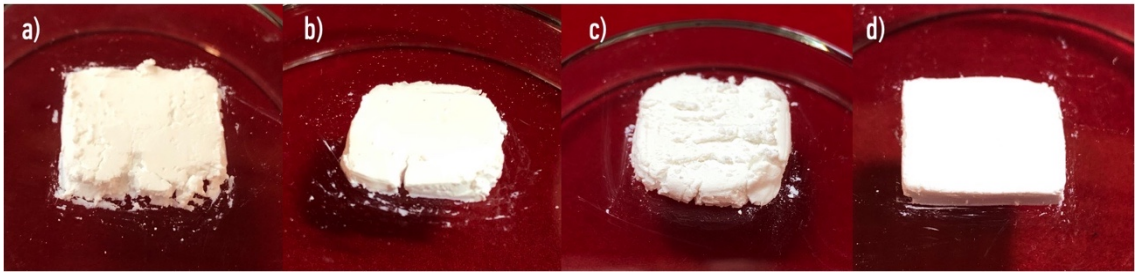

Figure 28 The wet cracking behavior of coagulated samples with a) AA100, b) AMPS100, c) VPA50, and d) the optimum additive, AMPS50

AA100 and VPA50 samples did not respond well to shaping, cutting through the material caused the cracks to form, and attempting to smoothen the surface caused the samples to split and break repeatedly with the movement, which is clear for VPA50-sample. The use of AMPS100 displayed a slightly better behavior in terms of the response to touching the surface but cracked under a small perpendicular pressure. On the other hand, the sample containing AMPS50 met the criteria of the characterization in that the product displayed no cracks despite the movements and forces exerted on it. In Figure 29, we chose AA100 to show that the presence of cracks is intensified after drying overnight to the point of complete breakage and failure, rendering the sample unsuitable for sintering. In contrast, the sample prepared with AMPS50 did not crack after drying overnight nor after sintering under the conditions described in section 3.2.8.

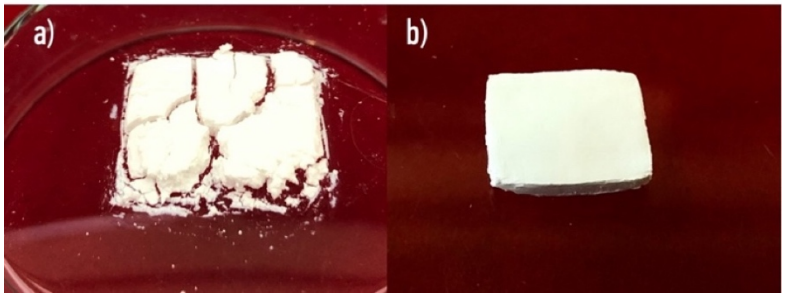

Figure 29 Comparison between the a) dry behavior of the sample containing AA100, and b) the sintered sample containing AMPS50

Since VPA50 displayed the worst case of malleability, we eliminated it from the moisture content measurements. The rest of the polymers were evaluated to study the water retention in the samples when left to dry at room temperature, the test was done on 65 wt. % suspensions, which is the maximum loading. The rate at which the moisture content was changing with time was the lowest in AMPS50 governed by the least steep slope, given in Figure 30. AA100 displayed the most drastic loss in water from the time of preparation, 45% loss occurred after 6 hours of drying. AMPS50 retained about 23% more water compared to both AMPS100 and AA100 after 6 hours of drying. At this point, we have proven that AMPS50 is the best performing linear copolymer as a coagulant in retaining the moisture, capable of being shaped without displaying cracking behavior under various movements.

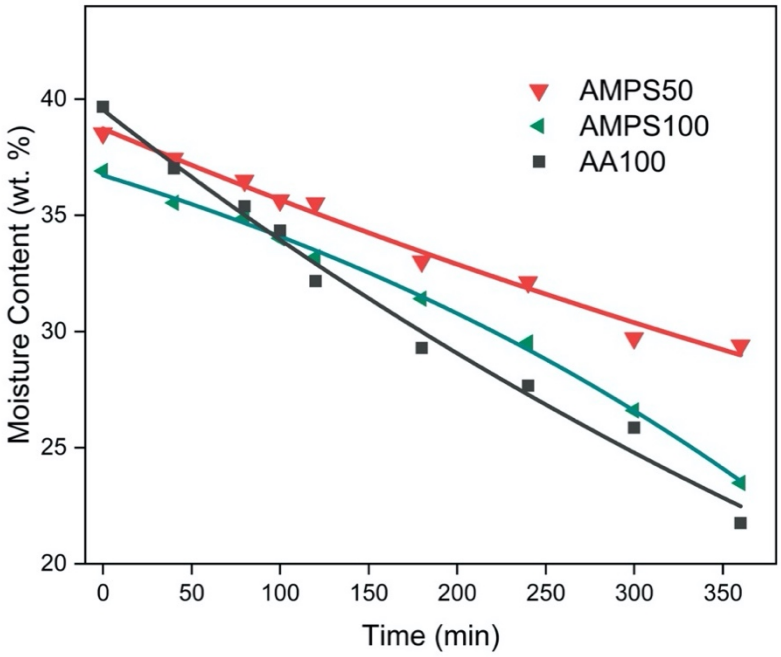

Figure 30 The moisture content of 65 wt. % YSZ suspensions dried at room temperature up to taking the measurement, then dried at 150 ˚C

3.3.5. The machinability in Wet and Dry States

To maintain a homogeneous, highly viscous, crack-free, and malleable YSZ formulation of 65 wt. % loading, we singled out AMPS50 at 1 wt. % due to its performance in wet, dry, and sintered states. This malleability was due to the dough-like consistency of the colloids that immediately occurred when AMPS50 was added to the system. The ease of forming and molding made it possible to penetrate the material in the wet state. Figure A1 shows a needle inserted in the dough where the material was sculpted into a rectangular rod. The induced hole was stable, did not cause the sample to break, and homogeneously spanned the rod end-to-end. Additionally, this method can be used for any size of the specimen, validating its reproducibility thereof. However, this technique is useful for applications that do not require accuracy on a millimeter scale. For such applications, drilling/machining using a sample holder and a drilling/lathe machine in the dry state is more precise. Figure A2 elucidates a ball that was shaped by hand and let to dry, the ball (14.7 mm diameter) was then drilled with a pin of 0.6 mm size, while dry at 8000 rpm. Sintering did not cause any cracking, which confirms the lack of it in the dry body as sintering extenuates cracks if they exist. The shrinkage of the

ball after sintering was about 22%, which was a common shrinkage rate of all the samples.

Using a lathe machine, we drilled one cylinder-shaped rod in its semi-wet state — the supporting visual material (video) illustrates the lathing machining. The result is as seen in Figure 31, showing the rod both before and after sintering. This specific shape is utilized for thermocouples that have conductive wires that require to be covered with an insulating material in this case, a ceramic. In contrast to the conventional ceramic processing methods for producing such tools, this technique is facile, easy-to-reproduce, and reliable.

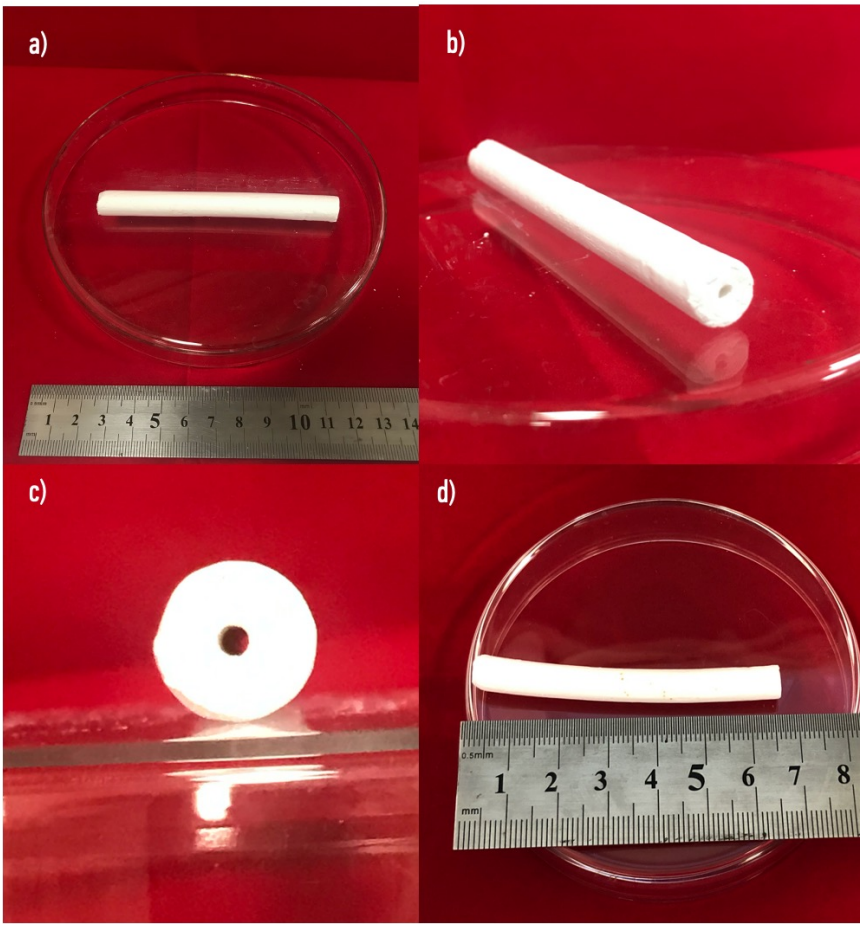

Figure 31 The drilled rod in dry green body state a lath machine with a pin of 2 mm diameter size and 16 cm length a) Top view of the dry body b) and c) cross-sectional view showing the hole size and dimensional stability d) the sintered rod showing shrinkage and slight deflection

3.3.6. Shrinkage, Density, and Mechanical Strength

The dimensional shrinkage of the samples was isotropic and was calculated to be 22.8%, which is comparable to the reported values in the literature [26, 48, 49]. Figure 17 demonstrates the size difference between the dry green body and the sintered body that was made using the same mold with a diameter of 1 cm. While wet, the sample takes the shape of the mold without any dimensional variation. During drying at room temperature with about 10% moisture loss, which is after 3 hours from the start according to Figure 30, the sample starts to exhibit slight drying shrinkage. When left overnight to dry, the sample shrinks about 8%. The density was found to be 5.92 and 5.93 which are 97.7% of the theoretical density of 3 mol YSZ, and it matches the density reported by the nanoparticles' manufacturer. On the other hand, the surface morphology of the sample showed a few pores, which can be attributed to the way the sample was shaped and handled. The lines are due to the polishing. The average mechanical strength of the sintered samples was recorded to be 149 MPa.

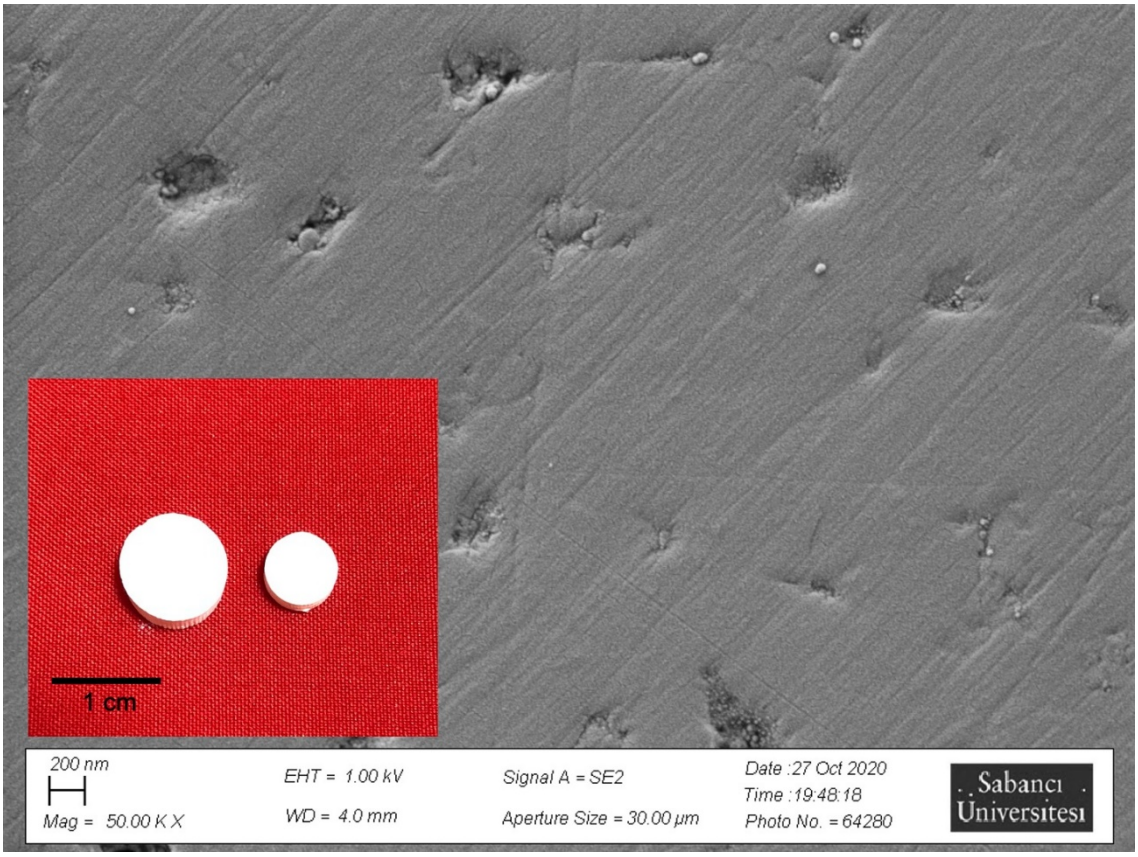

Figure 32 SEM micrograph of the surface morphology of the sintered pellet displayed on the right of the sample image.

3.4. Conclusion

The instant coagulation of the YSZ nanoparticles that results in i) sustained stabilization of the suspension in its fresh state ii) malleable dough at room temperature iii) crack-free homogeneous highly-viscosity consistency iv) machinable material, both the wet and the dry green bodies, can only be successfully attained by intricate tailoring of the coagulant properties to the type of the particle and its surface properties. This work provides an innovative approach to casting and processing 3 mol % yttria-stabilized zirconia at the minimum additive amount of 1 wt. %. This particle-specific design, governed by polymer-polymer bridging, facilitates the decrease of the required additive amount, which in turn eliminates post-processing steps in ceramic casting.

3.5. References

[1] F. Zhang *et al.*, "High-translucent yttria-stabilized zirconia ceramics are wear-resistant and antagonist-friendly," *Dent. Mater.*, vol. 35, no. 12, pp. 1776–1790, 2019.

[2] A. Selçuk and A. Atkinson, "Strength and toughness of tape-cast yttria-stabilized zirconia," *J. Am. Ceram. Soc.*, vol. 83, no. 8, pp. 2029–35, 2000.

[3] J. W. Adams, R. Ruh, and K. S. Mazdiyasni, "Young's modulus, flexural strength, and fracture of yttria-stabilized zirconia versus temperature," *J. Am. Ceram. Soc.*, vol. 80, no. 4, pp. 903–908, 1997.

[4] A. A. Briggs, W. A. Dench, and W. Slough, "A null-point solid electrolyte electrochemical cell for measuring low oxygen partial pressures at high temperatures," *J. Chem. Thermodyn.*, vol. 3, no. 1, pp. 43–49, 1971.

[5] W. Fan *et al.*, "Improved properties of scandia and yttria co-doped zirconia as a potential thermal barrier material for high temperature applications," *J. Eur. Ceram. Soc.*, vol. 38, no. 13, pp. 4502–4511, 2018.

[6] L. Tayebi, F. Sadaat Tabatabaei, and R. Torres, "Biomedical Materials in Dentistry," in *Applications of Biomedical Engineering in Dentistry*, 1st ed., Springer Nature Switzerland, 2020, pp. 3–20.

[7] C. Piconi and G. Maccauro, "Zirconia as a ceramic biomaterial," *Biomaterials*. 1999.

[8] T. Ketcham, W. R. Powell, R. Stewart, and J. St., “United States Patent,” 6045935, 2000.

[9] Y. Zhang, J. Gao, D. Peng, M. Guangyao, and X. Liu, “Dip-coating thin yttria-stabilized zirconia films for solid oxide fuel cell applications,” *Ceram. Int.*, vol. 30, no. 6, pp. 1049–1053, 2004.

[10] C. J. Elliott, M. J. Large, J. V. Pearce, and G. Machin, “Compatibility of Materials for Use at High Temperatures with W–Re Thermocouples,” *Int. J. Thermophys.*, vol. 35, pp. pages1202–1214, 2014.

[11] S. Mohanty, A. P. Rameshbabu, S. Mandal, B. Su, and S. Dhara, “Critical issues in near net shape forming via green machining of ceramics: A case study of alumina dental crown,” *J. Asian Ceram. Soc.*, 2013.

[12] P. Taylor, H. Hocheng, K. L. Kuo, and J. T. Lin, “Materials and Manufacturing Processes Machinability of Zirconia Ceramics in Ultrasonic Drilling Machinability of Zirconia Ceramics in Ultrasonic Drilling,” no. October 2012, pp. 37–41, 2011.

[13] G. Ma, S. Yan, D. Wu, Q. Miao, M. Liu, and F. Niu, “Microstructure evolution and mechanical properties of ultrasonic assisted laser clad yttria stabilized zirconia coating,” *Ceram. Int.*, vol. 43, no. 13, pp. 9622–9629, 2017.

[14] T. Kizaki, T. Ogasahara, N. Sugita, and M. Mitsuishi, “Ultraviolet-laser-assisted precision cutting of yttria-stabilized tetragonal zirconia polycrystal,” *J. Mater. Process. Technol.*, vol. 214, no. 2, pp. 267–275, 2014.

[15] Y. Ito, N. Sugita, T. Fujii, T. Kizaki, and M. Mitsuishi, “Precision machining of sintered zirconia ceramics by high-speed milling,” *Int. J. Autom. Technol.*, 2017.

[16] T. Kizaki, T. Kitaguchi, N. Sugita, and M. Mitsuishi, “Effect of machining parameters on precision machining of zirconia ceramics using heated cutting tools,” in *Conference Proceedings - 14th International Conference of the European Society for Precision Engineering and Nanotechnology, EUSPEN 2014*, 2014.

[17] R. Onler, E. Korkmaz, K. Kate, R. E. Chinn, S. V. Atre, and O. B. Ozdoganlar, “Green micromachining of ceramics using tungsten carbide micro-endmills,” *J. Mater. Process. Technol.*, vol. 267, no. 2, pp. 268–279, 2019.

[18] M. G. Holthaus *et al.*, “Micromachining of ceramic surfaces: Hydroxyapatite and zirconia,” *J. Mater. Process. Technol.*, vol. 214, no. 2, pp. 267–275, 2012.

[19] J. Yang, J. Yu, Y. Cui, and Y. Huang, “New laser machining technology of Al 2O 3 ceramic with complex shape,” *Ceram. Int.*, vol. 38, no. 5, pp. 3643–3648, 2012.

[20] S. Dhara and B. Su, “Green machining to net shape alumina ceramics prepared

using different processing routes," *Int. J. Appl. Ceram. Technol.*, vol. 2, no. 3, pp. 262–270, 2005.

[21] G. Avci, O. Akhlaghi, B. Ustbas, C. Ozbay, Y. Z. Menceloglu, and O. Akbulut, "A PCE-based rheology modifier allows machining of solid cast green bodies of alumina," *Ceram. Int.*, vol. 42, no. 3, pp. 3757–3761, 2016.

[22] A. Demarbaix, F. Ducobu, N. Preux, F. Petit, and E. Rivière-Lorphèvre, "Green ceramic machining: Influence of the cutting speed and the binder percentage on the Y-TZP behavior," *J. Manuf. Mater. Process.*, vol. 4, no. 2, pp. 1–10, 2020.

[23] F. T. Filser, "Direct Ceramic Machining of Ceramic Dental Restorations," *Ph.D. thesis. Zurich*, 2001.

[24] F. Filser, P. Kocher, and L. J. Gauckler, "Net-shaping of ceramic components by direct ceramic machining," *Assem. Autom.*, vol. 23, no. 4, pp. 382–390, 2003.

[25] M. Yang *et al.*, "Direct coagulation casting of alumina via controlled release of calcium from ammonium polyphosphate chelate complex," *J. Mater. Res.*, vol. 31, no. 1, pp. 154–162, 2016.

[26] K. Gan *et al.*, "In-situ coagulation of yttria-stabilized zirconia suspension via dispersant hydrolysis using sodium tripolyphosphate," *J. Eur. Ceram. Soc.*, vol. 37, no. 15, pp. 4868–4875, 2017.

[27] J. A. Lewis, "Colloidal Processing of Ceramics," *J. Am. Ceram. Soc.*, 2004.

[28] R. Moreno, "Colloidal processing of ceramics and composites," *Adv. Appl. Ceram.*, 2012.

[29] G. Tari, "Gelcasting ceramics: A review," *Am. Ceram. Soc. Bull.*, vol. 82, no. 4, pp. 43–46, 2003.

[30] S. Dhara and P. Bhargava, "Egg White as an Environmentally Friendly Low-Cost Binder for Gelcasting of Ceramics," *J. Am. Ceram. Soc.*, vol. 84, no. 3–12, pp. 3048–3050, 2001.

[31] J. Yang and Y. Huang, *Novel colloidal forming of ceramics*. 2020.

[32] L. J. Gauckler, T. J. GRAULE, F. H. BAADER, and J. WILL, "Colloidal processing of ceramics: direct coagulation casting," *Turkey . III Ceram. Congr. Proc. B.*, vol. 26, pp. 11–26, 1966.

[33] E. Ewais, A. A. Zaman, and W. Sigmund, "Temperature induced forming of zirconia from aqueous slurries: Mechanism and rheology," *J. Eur. Ceram. Soc.*, 2002.

[34] Y. Dong, X. Li, S. Liu, J. G. Li, and X. Sun, "Novel direct coagulation casting of alumina suspensions using Y 3+-ion releasing substances as coagulant," *Key Eng. Mater.*, vol. 602–603, pp. 164–169, 2014.

[35] T. Graule, F. H. Baader, L. J. Gauckler, and T. J. . B. Graule F.H.;Gauckler, L.J., "Shaping of ceramic green compacts direct from suspensions by enzyme catalyzed reactions," *cfi/Ber. DKG*, vol. 71, no. 6, pp. 317–323, 1994.

[36] T. Tridib and D. Bhudeb R., "Flocculation : A New Way to Treat the Waste Water," *J. Phys. Sci.*, vol. 10, pp. 93–127, 2006.

[37] R. Hogg, "Bridging flocculation by polymers," *KONA Powder and Particle Journal*. 2012.

[38] S. Biggs, "Steric and Bridging Forces between Surfaces Bearing Adsorbed Polymer: An Atomic Force Microscopy Study," *Langmuir*, vol. 11, no. 1, pp. 156–162, 1995.

[39] H. N. W. Lekkerkerker and R. Tuinier, "Stability of colloid-polymer mixtures," in *Lecture Notes in Physics*, Dordrecht: Springer, 2011.

[40] J. B. Hooper and K. S. Schweizer, "Contact aggregation, bridging, and steric stabilization in dense polymer-particle mixtures," *Macromolecules*, vol. 38, no. 21, pp. 8858–8869, 2005.

[41] J. Plank and O. T. Salami, "Synthesis, Effectiveness, and Working Mechanism of Humic Acid-{sodium 2-acrylamido-2-methylpropane sulfonate-co-N,N-dimethyl acrylamide-co-acrylic acid} Graft Copolymer as High-Temperature Fluid Loss Additive in Oil Well Cementing," *J. Appl. Polym. Sci.*, vol. 126, no. 4, pp. 1449–1460, 2011.

[42] J. Chevalier, S. Deville, E. Münch, R. Jullian, and F. Lair, "Critical effect of cubic phase on aging in 3 mol% yttria-stabilized zirconia ceramics for hip replacement prosthesis," *Biomaterials*, vol. 25, no. 24, pp. 5539–5545, 2004.

[43] S. Paul, "Biomedical engineering and its applications in healthcare," in *Biomedical Engineering and its Applications in Healthcare*, Springer, 2019, pp. 1–738.

[44] Z. Goharibajestani *et al.*, "Incorporating steric hindrance into the additive design enables a robust formulation of alumina ink for extrusion-based 3d printing," *ACS Appl. Polym. Mater.*, 2019.

[45] A. International, "Standard Test Method for Flexural Strength of Advanced Ceramics at Ambient," *Order A J. Theory Ordered Sets Its Appl.*, vol. 94, no. Reapproved, pp. 1–15, 1996.

[46] J. Xu, K. Gan, M. Yang, Y. Qu, J. Wu, and J. Yang, "Direct coagulation casting of yttria-stabilized zirconia using magnesium citrate and glycerol diacetate," *Ceram. Int.*, vol. 41, no. 4, pp. 5772–5778, 2015.

[47] D. Ghernaout, "Controlling Coagulation Process: From Zeta Potential to Streaming Potential," *Am. J. Environ. Prot.*, vol. 4, no. 5, p. 16, 2015.

[48] K. Chen, Y. Tian, Z. Lü, N. Ai, X. Huang, and W. Su, “Behavior of 3 mol% yttria-stabilized tetragonal zirconia polycrystal film prepared by slurry spin coating,” *J. Power Sources*, vol. 186, no. 1, pp. 128–132, 2009.

[49] D. A. Komissarenko, P. S. Sokolov, A. D. Evstigneeva, I. A. Shmeleva, and A. E. Dosovitsky, “Rheological and curing behavior of acrylate-based suspensions for the DLP 3D printing of complex zirconia parts,” *Materials (Basel).*, vol. 11, no. 12, 2018.

APPENDIX

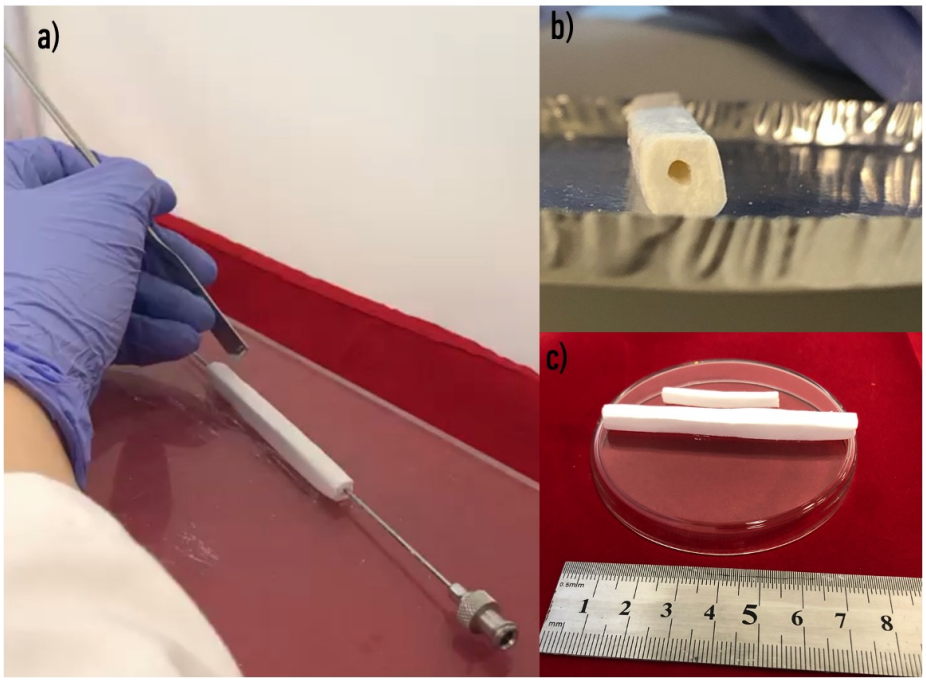

Figure A1 Wet State Formability a) During forming, b) cross-section of the hole c) Reproducibility of different sizes

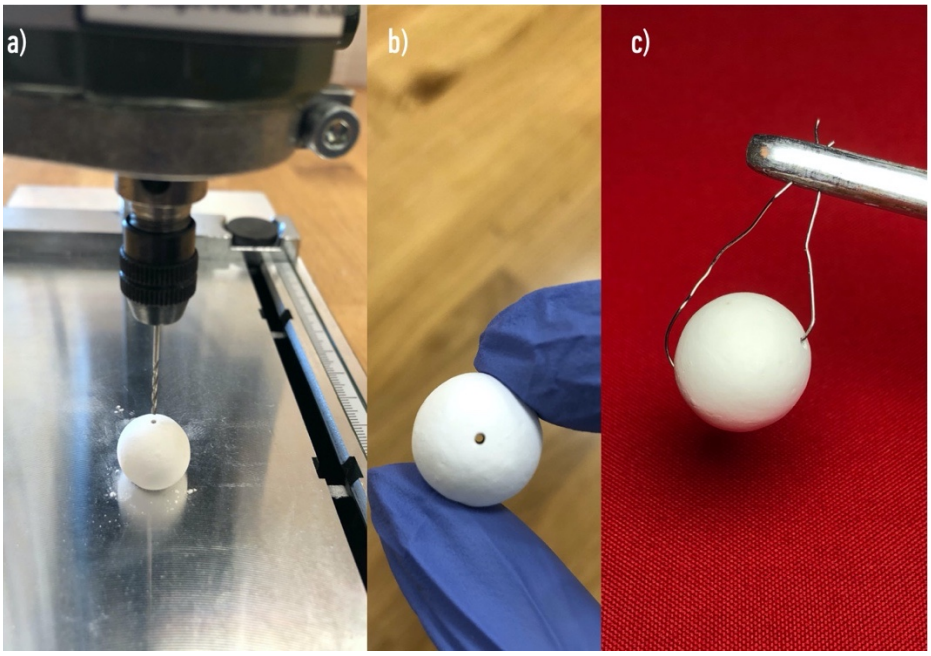

Figure A2 Dry Green Body State Machinability a) Right after drilling, b) Cross-section of the ball and the drilled hole of size 0.6 mm, c) the final sintered ball encircling a wire